Master of Science

# 전고체리튬전지용 Ag 도핑된 NASICON 유형의 $Li_{1.3}Al_{0.3}Ti_{1.7}(PO_4)_3$ 고체전해질의 이온전도도와 전기화학적 성능 연구

# Ionic conductivity and electrochemical performance of silver-modified NASICON-type $Li_{1.3}Al_{0.3}Ti_{1.7}(PO_4)_3$ solid electrolyte for all-solid-state lithium batteries

The Graduate School of University of Ulsan

Department of Chemistry

Luhur Muhammad Sadewo Panghudi

전고체리튬전지용 Ag 도핑된 NASICON 유형의 $Li_{1.3}Al_{0.3}Ti_{1.7}(PO_4)_3$

고체전해질의 이온전도도와 전기화학적 성능 연구

# Ionic conductivity and electrochemical performance of silver-modified NASICON-type $Li_{1.3}Al_{0.3}Ti_{1.7}(PO_4)_3$ solid electrolyte for all-solid-state lithium batteries

Supervisor : Professor Kwang-Sun Ryu

This dissertation was submitted to
The Graduate School of University of Ulsan
In partial fulfillment of the requirements for the degree of

**Master of Scince**

Luhur Muhammad Sadewo Panghudi

Department of Chemistry

University of Ulsan, South Korea

December 2020

Ionic conductivity and electrochemical performance of silver-modified NASICON-type $Li_{1.3}Al_{0.3}Ti_{1.7}(PO_4)_3$ solid electrolyte for all-solid-state lithium batteries

This certifies that the dissertation of
Luhur Muhammad Sadewo Panghudi is approved

Committee Chair Professor Jaehoon Jung

Committee Member Professor Eun Seok Oh

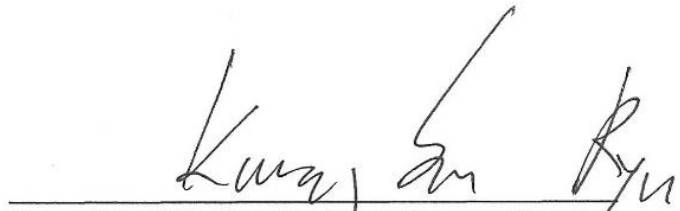

Committee Member Professor Kwang-Sun Ryu

Department of Chemistry
University of Ulsan, South Korea
December 2020

# Acknowledgements

No word can describe my gratitude and gratefulness for what I have achieved by this time. First of all, I praise to Allah SWT for the blessing and the ease of being able to complete this project. I would like to thank my beloved parents who always give unlimited love in my life, and always supported me by giving the best they had. It feels like just yesterday, I was so excited to go to Korea to start a new adventure and face the challenges approaching ahead. These 2 years I have spent here gave me a bunch of life experience and new lesson learn, especially about survival in another country and willing to learn to study far away from family.

My heartfelt gratitude to my supervisors, Prof. Kwang-Sun Ryu for his valuable advices, guidance, constant supports, and his dedication who has allowed me to learn and being part of the SMDL group where I learned new things which certainly will be useful for me in the future, also he taught me about persistence in learning and innovating. I would like to express my sincere gratitude to Dr. Rajesh and Dr. Yuva for their help during my studies and laboratory experiments, it feels so hard without your helpful discussion and advice. I also would like to thank my senior, Young Jin who taught me the basics of using tools in the laboratory. Thank you to Suyeon who always listened to my story on campus and also helps me with many things, especially for SEM analysis and using Origin.

Last but not least, I would like to thank my SMDL buddy who was very good at accepting me even though I was the only foreign student at that time Thank you to Minho who is never tired to help and provide useful input on my work so I can graduate together and always provides me a piece of important information related to lectures and graduation, thank you for all your help and kindness. Thanks to Jiwoon who always smile and kind, even though in a panic condition and very polite for anything and always be there when I need help. Thanks to

Sujeong who helped me to improve my Korean language while on campus and listened to my stories from life stories to KPOP. Thank you to Hakmin who smiled generously and became a chair matte on the bus when I got home early, Wish we can sing again in another time. Thanks to Geumji who always kind and gracious to all people. Also, thanks to Ms. Hyuna, the super hardworking woman for taking her master course while working in a company and always kind to me. I could not be more grateful for all your kindness, warmth, and love for me. May God repays all of your kindness, stay healthy, wealthy, gorgeous, and hope we can meet again someday.

# Abstract

Recently, all-solid-state lithium batteries have received attention because of the electrochemical performance, safety, and reliability as well as high energy densities. NASICON-type $Li_{1.3}Al_{0.3}Ti_{1.7}(PO_4)_3$ (LATP) oxide-based solid electrolyte shows the favorable mechanical property, high $Li^+$ transfer number, and excellent electrochemical and thermal stability. Water-soluble binders were introduced in order to increase the ionic conductivity of LATP. Silver was successfully substituted to the LATP solid electrolyte using a modified solid-state method for all-solid-state lithium batteries (ASSLBs). The pristine LATP was also synthesized for comparison before and after silver modification. The water-soluble binders was added to the mixture of solid electrolyte before sintering process to increase the ionic conductivity of solid electrolyte. The XRD, SEM, and EDS mapping confirmed the structural properties of LATP and silver-modified LATP $Li_{1.3}Al_{0.4}Ag_{0.1}Ti_{1.6}(PO_4)_3$. X-ray diffraction patterns showed the peak shifting after the addition of various binders were shown as the effect of the binders on the electrolyte. A similar peak with slightly increased and peak broadening for silver-modified LATP appeared after the addition of silver. There are also a small new peak appeared at around 46.5° theta degree indicating that the modification of silver on LATP has successfully synthesized. The ionic conductivity measurement was conducted by Electrochemical Impedance Spectroscopy (EIS) and revealed LATP with 1% PVA is currently displaying a highest value of $4.65 \times 10^{-5}$ S/cm as binder for solid electrolytes. Cyclic voltammetry and DC-cycling for those solid electrolyte was measured to observe the stability of electrolyte against Li metal, and it revealed that the addition of water-soluble binders may improve the electrochemical stability of the solid electrolytes.

# Contents

## Chapter 2. General experimental



## Chapter 3. Effect of water-soluble binders on the synthesis of LATP and silver-modified LATP $Li_{1.3}Al_{0.4}Ag_{0.1}Ti_{1.6}(PO_4)_3$ solid electrolytes

# List of Tables

# List of Figures

**Figure 3.1** Schematic illustration for synthesis procedure of LATP and silver-modified LATP solid electrolyte.

**Figure 3.2** Schematic illustration of (a) press cell for EIS (b) Solid electrolyte pellet, and coin cell assembly configuration for (c) cyclic voltammetry and (d) DC-cycling.

**Figure 3.3** XRD Pattern of LATP ($Li_{1.3}Al_{0.3}Ti_{1.7}(PO_4)_3$) with different water-soluble binders (left) and magnified reflections around $2\theta = 33.3°$ showing a peak shifting from (a) LATP before addition of binders and LATP with water-soluble binders (b) 1% PVA, (c) 1% CMC and (d) 1% PAA.

**Figure 3.4** SEM images of (a) $Li_{1.3}Al_{0.3}Ti_{1.7}(PO_4)_3$ solid electrolyte, (b) Mapping results of electrolytes, and (c) EDS mapping of $Li_{1.3}Al_{0.3}Ti_{1.7}(PO_4)_3$ with water-soluble binders with general mapping, Al, Ti, P, and O mapping with 10μm scale images.

**Figure 3.5** Nyquist plot of $Li_{1.3}Al_{0.3}Ti_{1.7}(PO_4)_3$ with various binders in In | solid electrolytes | In symmetric cell at room temperature.

**Figure 3.6** (a-d) Cyclic voltammetry for LATP and water-soluble binders LATP materials at a scan rate of 1mV/s from -0.5 V to 5 V from the Li/electrolyte/SUS cell

**Figure 3.7** (a-d) Results of DC-cycling test of LATP and water-soluble added to LATP in the symmetric cells Li/solid electrolyte/Li with applied current density of 1 mA $cm^{-2}$ for 100 hours.

**Figure 3.8** XRD Pattern of LATP ($Li_{1.3}Al_{0.3}Ti_{1.7}(PO_4)_3$) and silver-modified LATP compared to the reference code of targeted material ($LiTi_2(PO_4)_3$) (a). This graph shows that the addition of silver to the LATP material did not show a significant difference with original material, but there is another peak formed at 46-47 theta degree and the addition of silver slightly increase the peak broadening (b-c).

**Figure 3.9** XRD Pattern of silver-modified LATP ($Li_{1.3}Al_{0.4}Ag_{0.1}Ti_{1.6}(PO_4)_3$) with different water-soluble binders (left) and magnified reflections around $2\theta = 44.5°$ and 47.7° showing a peak shifting from (a) $Li_{1.3}Al_{0.4}Ag_{0.1}Ti_{1.6}(PO_4)_3$ and $Li_{1.3}Al_{0.4}Ag_{0.1}Ti_{1.6}(PO_4)_3$ after addition binders of (b) 1% PVA, (c) 1% CMC and (d) 1% PAA. PDF 035-0754 as the reference code of targeted material ($LiTi_2(PO_4)_3$) also attached for comparison.

**Figure 3.10** SEM images of (a) $Li_{1.3}Al_{0.4}Ag_{0.1}Ti_{1.6}(PO_4)_3$ solid electrolyte, (b) EDS mapping of $Li_{1.3}Al_{0.4}Ag_{0.1}Ti_{1.6}(PO_4)_3$ with water-soluble binders with general mapping, Al, Ti, P, O, and Ag mapping with 25μm scale images, and (c) Mapping results of the electrolytes.

**Figure 3.11** Nyquist plot of $Li_{1.3}Al_{0.4}Ag_{0.1}Ti_{1.6}(PO_4)_3$ with various binders in In |solid electrolytes | In symmetric cell at room temperature.

**Figure 3.12** (a-d) Cyclic voltammetry for $Li_{1.3}Al_{0.4}Ag_{0.1}Ti_{1.6}(PO_4)_3$ and water-soluble binders $Li_{1.3}Al_{0.4}Ag_{0.1}Ti_{1.6}(PO_4)_3$ materials at a scan rate of 1mV/s from -0.5 V to 5 V from the Li/electrolyte/SUS cell.

**Figure 3.13** (a-d) Results of DC-cycling test of $Li_{1.3}Al_{0.4}Ag_{0.1}Ti_{1.6}(PO_4)_3$ and water-soluble added to $Li_{1.3}Al_{0.4}Ag_{0.1}Ti_{1.6}(PO_4)_3$ in the symmetric cells Li/solid electrolyte/Li with applied current density of 1 mA $cm^{-2}$ for 100 hours.

# Chapter 1. Introduction

## 1-1. Lithium secondary batteries

Lithium secondary batteries are electrochemical devices that can store energy by converting chemical energy into electrical energy through chemical reactions in the system and using electrolytes that channel lithium ions when ion is displaced. This device allows ion displacement to be reversible when given a voltage and the redox reactions are repeated within the same electrode hence this devices can be recharged repeatedly for rechargeable batteries. The first rechargeable lithium ion batteries were introduced by Sony Corporation in 1991 and still become a common portable energy storage devices in recent times. There are numerous rechargeable batteries were developed such as lithium ion batteries, lead-acid batteries, Ni-Cd batteries, Ni-MH batteries, lithium metal batteries, and so on. Figure 1.1 shows the different shape of lithium secondary battery that currently fabricated. In addition, lithium ion batteries show a high energy and power densities (up to 200 Wh $Kg^{-1}$) among other rechargeable batteries since lithium is the most electropositive as well as the lightest metal (-3.05 V versus standard hydrogen electrode), thus facilitating the design of storage systems with high energy density. The advent of plug-in hybrid electric vehicles (PHEVs) and electric vehicles (Evs) has brought greater attention to lithium secondary batteries, which have higher energy and output compared to NiMH cells as shown in Figure 1.2 [1, 2]. However, lithium ion batteries still have some problem in safety while leaking which cause thermal runaway and explosion due to the use of organic electrolyte which is not stable in air. To overcome this dangerous risk, researchers tried to develop a new material composition and systems with same characteristics yet safer than the previous lithium ion batteries.

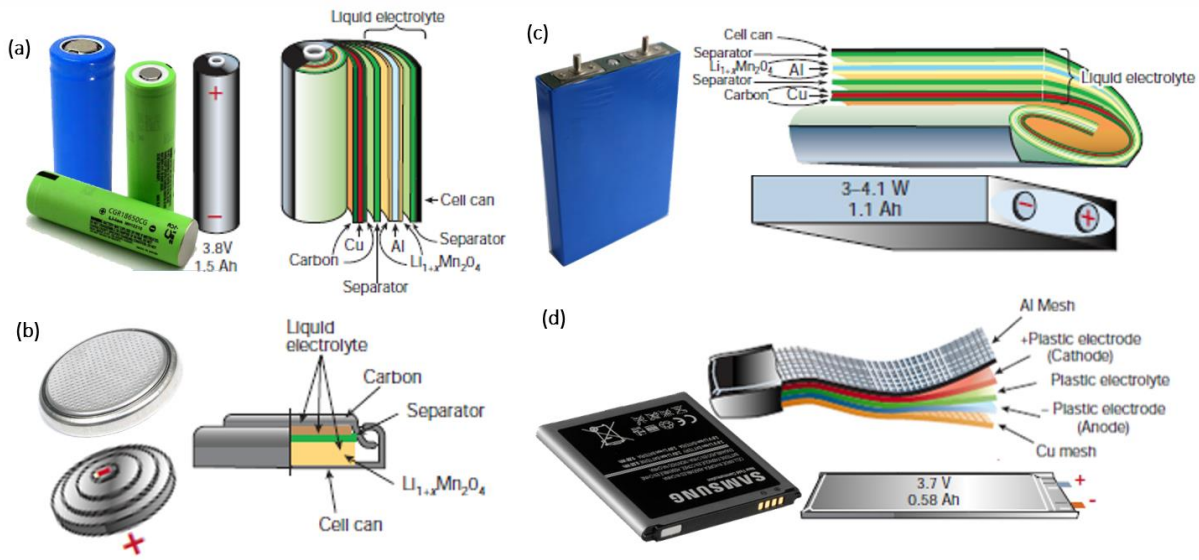


**Figure 1.1** Different shapes of lithium secondary batteries: (a) cylindrical (b) coin (c) prismatic and (d) pouch [1].

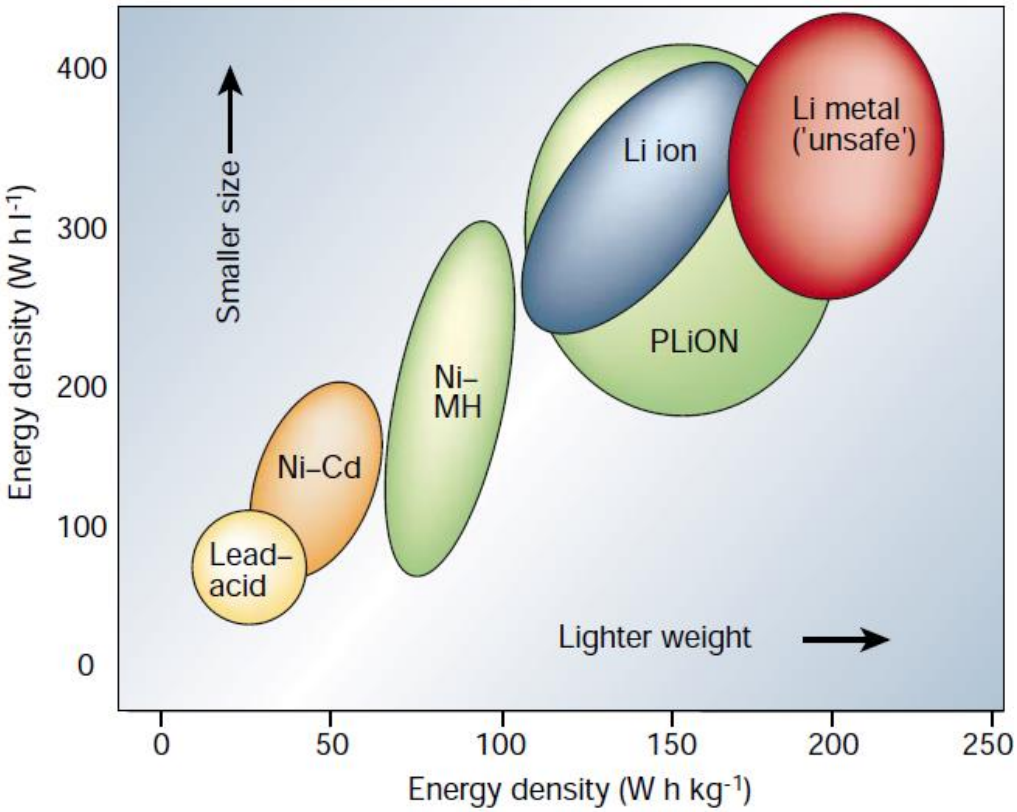


**Figure 1.2** Comparison of the different battery technologies in terms of volumetric and gravimetric energy density [2].

## 1-1-1. Composition of lithium secondary batteries

The composition of lithium secondary batteries basically composed by cathode, anode, electrolyte, and separator. The Cathode for Lithium Secondary Battery mostly fabricated by transition metal oxide materials, which can undergo oxidation to higher valences when lithium is removed [3]. This cathode materials involving intercalation and extraction of lithium ion with olivine, layered, and spinel structure as shown in Figure 1.3 [4]. Currently $LiCoO_2$ and $LiFePO_4$ are most widely used in commercial Li-ion batteries because of their good cycle life (>500 cycles) [5] and the properties of various cathode materials used in commercial lithium ion batteries are listed in Table 1.1 [1]. The anode materials are normally carbonaceous materials, which have large lithium storage capability and lead to a lower cell voltage. Anode donates electrons to the external circuit as the cell discharges and Li ion move through electrolytes, then it generate electricity. Another non carbonaceous anode also used for lithium batteries such as $Li_4Ti_5O_{12}$ (LTO), $Li_{4.4}Ge$, transition metal oxides, and so on. The electrolyte is a solution of lithium salt (e.g. $LiPF_6$) mixed with organic solvent (e.g. ethylene carbonate-dimethyl carbonate, EC-DMC) are used due to its high ionic conductivity and broad stability of voltage window (0-4.5V vs. $Li/Li^+$). Separators made of polymers or ceramics have a high-temperature melt integrity, which prevents short circuits caused by electrical contact between the cathode and the anode. Polyethylene, polypropylene and PVdF are commonly used as separator for lithium ion batteries [6].

## 1-1-2. Principle of lithium secondary batteries

Figure 1.4 shows the operating principle of typical lithium secondary battery. Rechargeable means the lithium transfer between cathode and anode through separator will remain repeating when the battery in charging or discharging state. The chemical reactions during charging and

discharging can be describe through this reaction as follows:

Cathode : $Li_{1-x}MO_2 + xLi^+ + xe^- \leftrightarrow LiMO_2$ (1.11)

Anode : $Li_xC \leftrightarrow C + xLi^+ + xe^-$ (1.12)

Overall : $Li_{1-x}MO_2 + Li_xC \leftrightarrow C + LiMO_2$ (1.13)

Charge neutrality occurs when ions flowing into electrodes collide with electrons entering through a conductor, thus forming a medium to store electric energy in the electrodes. Furthermore, the rate of reactions is increased as ions from the electrolyte are drawn to the electrodes. When charging, lithium ions are de intercalated from the layered $LiCoO_2$ intercalation host, pass across the electrolyte, and are intercalated between the graphite layers in the anode (Figure 1.5). When discharging, the reverse process occurs. The electrons, of course, pass around the external circuit. The electrode structure should be kept stable during the insertion and extraction of ions within electrodes, while an electrolyte acts as an ion transfer medium. The chemical energy made by the chemical reaction can be converted and stored to electronic energy by followed Nernst equation:

$$\Delta G = -nFE \quad (1.14)$$

Where G is Gibbs energy, n is number of electrons, F is Faraday`s constant number, and E is electric potential. This equation means that electric potential energies are proportional to chemical energies, which means that large chemical potential difference between cathode and anode induce large electric potential and energy. The electric potential proportioning to chemical energies is called to open circuit voltage (OCV) and is determined within the band gap of the electrolyte, which is determined energy difference between the highest occupied molecular orbital (HOMO) and the lowest unoccupied molecular orbital (LUMO) of the electrolyte in Figure 1.6 [2, 7-9].

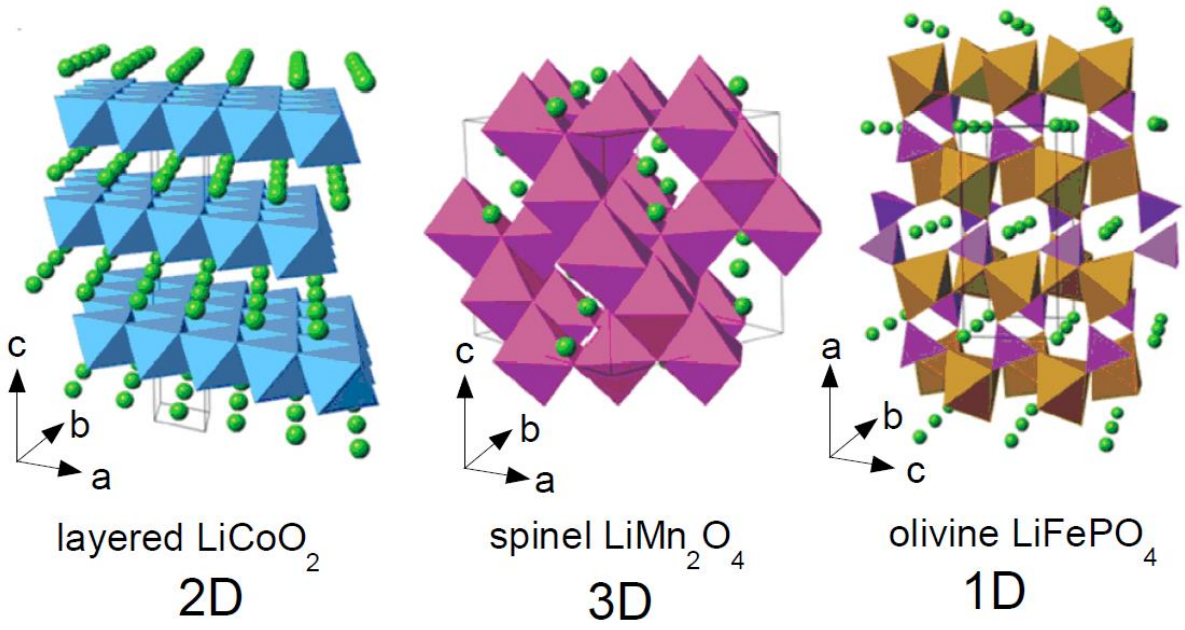


**Figure 1.3** Crystal structure of the three lithium-insertion compounds in which the $Li^+$ ions are mobile through the 2-D (layered), 3-D (spinel) and 1-D (olivine) frameworks [4].

**Table 1.1.** Properties of various cathode materials used in commercial Lithium Ion Batteries. [1]

| Cathode Material | Midpoint voltage vs Li (C/20) | Specific Capacity (Ah/kg) | Advantages | Disadvantages | Applications |
|---|---|---|---|---|---|
| $LiCoO_2$ **(LCO)** | 3.9 | 155 | In common use :<br>• Good cycle life<br>• Good energy | Moderate charged state thermal stability | Mainly smaller portable electronics (3C) |
| $LiMn_2O_4$ **(LMO)** | 4.0 | 100-122 | • Very good thermal stability<br>• Inexpensive<br>• Very good power capability | • Moderate cycle life<br>• Lower energy | Higher power applications such as power tools and electric motive power |
| $LiNi_{0.8}Co_{0.15}O_2$ **(NCA)** | 3.7 | 180 | • Very good energy<br>• Good power capability<br>• Good cycle life | • Moderate charged state thermal stability<br>• Sensitive to moisture even in discharged state | Excellent for motive power and premium electronic applications |
| $LiNi_xMn_yCo_{1-x-y}O_2$ **(NMC)** | 3.8 | 160 | Very good combination of properties (energy, power, cycle life, and thermal stability) | Patent issues | Both portable and high power applications including power tools and electric vehicles |
| $LiFePO_4$ **(LFP)** | 3.4 | 160 | • Very good thermal stability and cycle life<br>• Good power capability | • Lower energy<br>• Special preparation conditions | Mainly used in high power such as power tools and energy storage applications, patent issues |

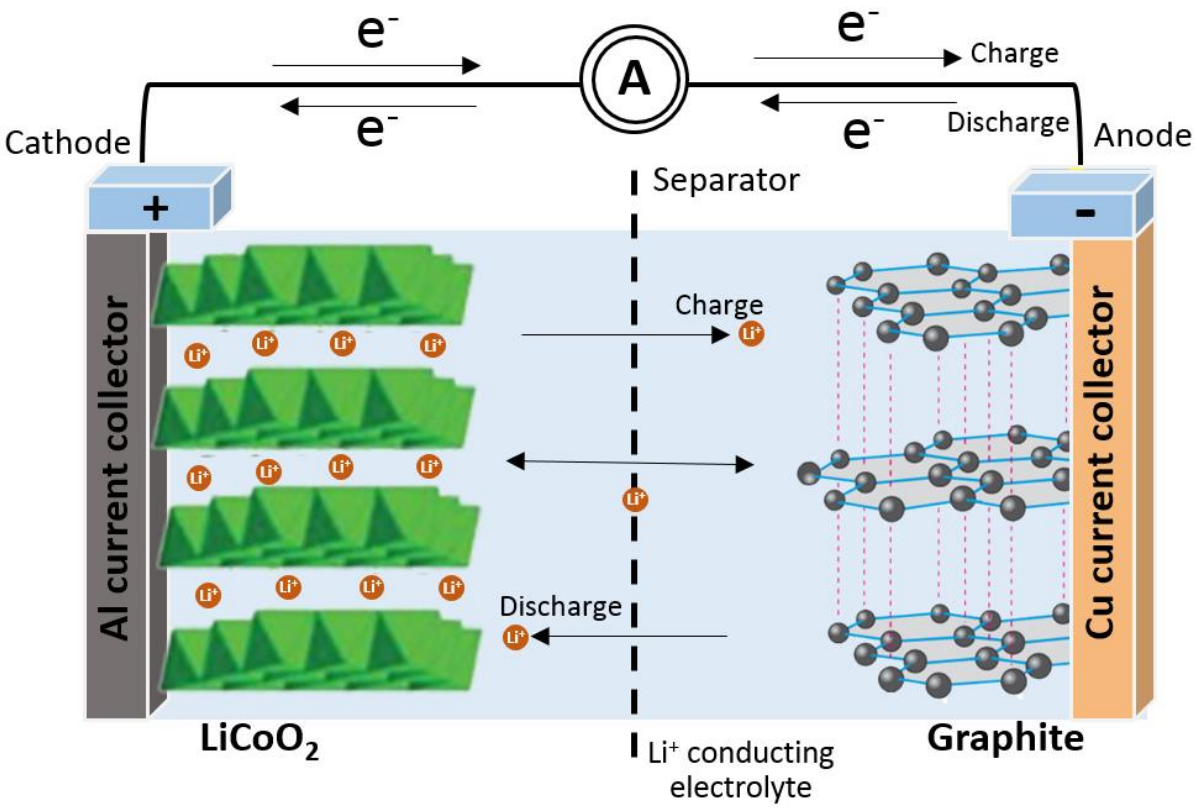


**Figure 1.4** Schematic design of charge-discharge mechanism of $Li^+$ movement in an electrolyte and insertion/extraction of $Li^+$ within electrodes in a lithium secondary battery.

$$LiCoO_2 \leftrightarrow 0.5Li^+ + 0.5e^- + Li_{0.5}CoO_2$$

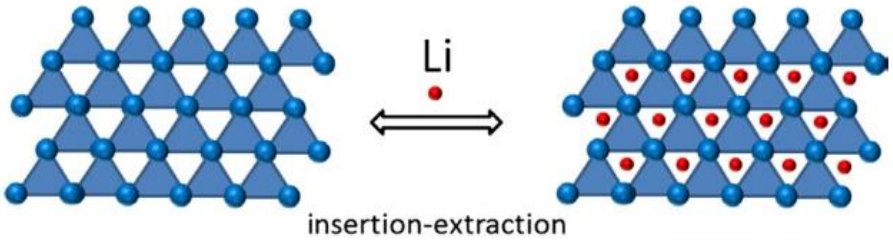


**Figure 1.5** Lithium insertion - extraction process on lithium secondary battery system.

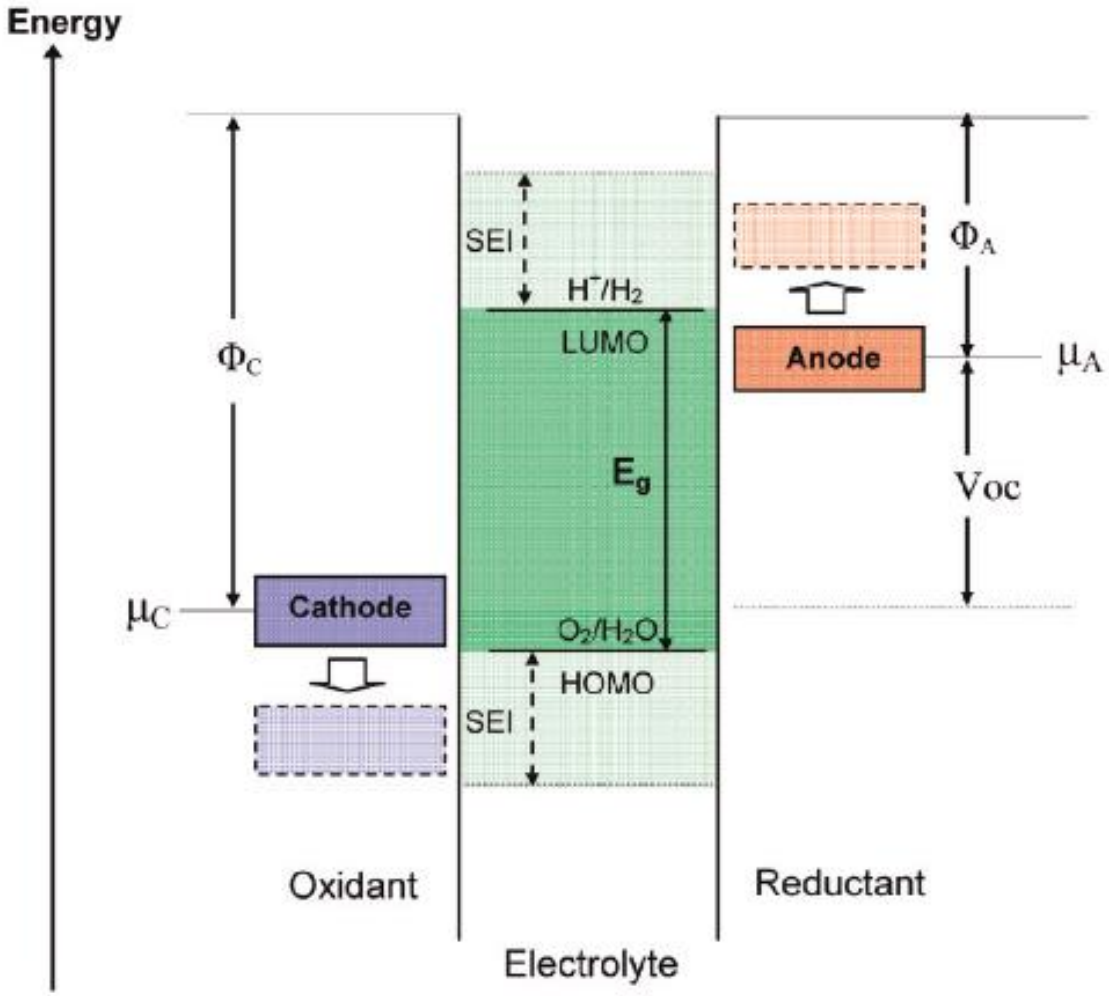


**Figure 1.6** Schematic open-circuit energy diagram of a lithium cell [9].

## 1-1-3. Properties and limitation of organic liquid electrolyte

There are numbers of electrolyte additives available for the Li-ion batteries. Commercial organic liquid electrolytes consist of a mixture of two or more carbonate-based materials and a lithium salt such as ethyl carbonate (EC)/di-methyl carbonate (DMC)=1:1 in 1M $LiFP_6$. The electrolytes have been applied to many lithium-based batteries due to its good dielectric constant and electrochemical stability compare with aqueous electrolyte. But, in order to be applied to a large scale energy devices, the electrolytes must be satisfy several requirements such as: [10]

1) Retention of the SEI during charge and discharge.
2) A $Li^+$ ion conductivity $\sigma_{Li} > 10^{-4} S/cm$.
3) An electronic conductivity $\sigma_e < 10^{-10} S/cm$.
4) A transference number $\sigma_{Li}/\sigma_{total} \approx 1$, where $\sigma_{total}$ includes conductivities by other ions in the electrolyte.
5) Chemical stability over wide temperature ranges.

Among these requirements, there are conditions that the organic electrolyte not meet such as low transference number, chemical stability, and electrochemical stability. Usually, lithium salt electrolytes have showed a low transference number of lithium ions (0.3~0.5/l) which occur a poor high-rate performance and limits the powder output of the cell [8] because of their dielectric mechanism such as solvation and dissociation. However, the most important thing to solve is safety related with thermal stability and leakage of the liquid types. As the organic electrolytes are decomposed and occur high thermal energy at high temperature, the lithium batteries expand and induce shrinkage of the membrane. And finally, the short between cathode and anode occurs and leads to explosion. To solve these problem, various type of electrolytes have been developed such as gel-type and solid state electrolyte due to their no leak properties and good thermal and electrochemical stability.

## 1-2. All-solid-state lithium ion batteries

Lithium-ion batteries have been widely used as rechargeable power sources for portable electronics and large-scale devices such as cell phones, laptop computers and hybrid electronic vehicles [11]. Usually, the traditional organic liquid electrolytes used in lithium ion batteries come with serious problems due to risks of leakage and flammability [12]. Therefore, the replacement of liquid electrolytes with a solid electrolyte could enhance the electrochemical performance, safety, reliability of these batteries as well as give a higher energy density [13]. Moreover, solid electrolytes have received much interest due to their potential for good ionic conductivity and a high lithium transference number (~1) compared to aprotic electrolytes (0.2~0.5) [10, 14] Among these advantages, the solid electrolytes for large scale electric devices have been intensively studied due to its attractive advantages for safety of lithium secondary batteries such as its electrochemical and thermal stability [2, 8]. The solid electrolytes are widely divided into ceramics and polymers. In the case of polymer electrolytes, they have good flexibility and also can be flexible batteries and devices. However, the poor mechanical properties and low ionic conductivity offset these electrolytes from practical applications. Therefore, many researchers have been studying ceramic solid electrolytes.

### 1-2-1 Ceramic solid electrolytes

Compare with the polymer electrolytes, ceramic solid electrolytes have been studied actively due to not only their good safety including strong mechanical strength and good ionic conductivity. There are many kinds of the electrolytes such as lithium hydrides, perovskites, lithium nitrides, LISICON-like (lithium superionic conductor), NASICON-like (sodium superionic conductor), argyrodites, and garnet [15]. As the powerful advantages, one of the ceramic electrolytes, lithium phosphorus oxynitride (LIPION), was applied to lithium secondary batteries as ceramic electrolyte for high temperature electric vehicle respectively [9].

## 1-2-2. Properties of ceramic solid-state electrolytes

The ceramic solid electrolytes meet followed requirements before they can be commercialized.

1) Strong mechanical strength
2) Chemical stability from thermal decomposition [9] and flammable [16].
3) High ionic conductivity due to high lithium transference number (~1) compared to aprotic electrolytes (0.2-0.5) [10].
4) Stable electrochemical stability window [17].
5) Good compatibility with lithium metal batteries due to its Li dendrite suppression properties [16].
6) Eco-friendly comparing with organic carbonate base electrolytes.

Almost the ceramics satisfy mechanical strength, chemical stability, nonflammable, Li dendrite suppression, and eco-friendly. Especially, the enhanced stability and safety of solid ceramic electrolyte provides new design of current solid-state battery cell simply and easily. Also, the solid electrolytes have high lithium transference number ($\sigma_{Li}/\sigma_{total}$) reducing the effects of concentration polarization from precipitations of the dissolved salt at the anode and depletion at the cathode [10] as the electrolyte is only worked by $Li^+$ migration compare with the liquid electrolytes including aprotic and lithium salt ions. As the results, lithium secondary battery lifetime and safety are increased [15]. The electrochemical stability window of many ceramic electrolytes is also known stable and wide. Almost the oxide electrolytes showed stable cathodic stability at the voltage window of cathode (5~9V versus $Li^+/Li$) and not induce self-decomposition during charge-discharge operation unlike the liquid organic electrolytes [10]. Consequently, the solid electrolytes can suppress repetition of SEI formation and $Li^+$ consumption, and finally increase life time of lithium secondary batteries.

### 1-2-3. $Li^+$ diffusion mechanism of ceramic solid electrolyte

Ceramic solid-state electrolytes are composed with not only mobile ions such as $Li^+$ but also nonmetal ligands forming polyhedral (4, 6, 8, and 12-fold coordination) and centered metals, which build the skeleton of the crystal structures. The polyhedra is regularly ordered by sharing such as corner or edge sharing and forms the $Li^+$ tunnel called bottleneck with interstitial between large anions and vacancy from not perfect crystallinity of solid materials due to thermodynamical stabilization [10, 18, 19]. The lithium ions are diffused by migration through the bottleneck in the crystal structures, while the liquid electrolytes involve moving solvated lithium ions in the solvent medium [10]. The migration is divided into Schottky and Frenkel migration. In the case of Schottky migration, the lithium ions migrate to the vacancy sites randomly. On the contrary, Frenkel migration is operated when lithium ions are diffused to direct interstitial between anions and exchange interstitial site [15]. Compare with the activation energy of the migration, Frenkel migration mechanism requires lower activation energy than Schottky migration. As the results, the $Li^+$ conductivity is depended on size and number of bottleneck [20]. Interstitial, and vacancy sites [21] which reliance on the lattice parameters of unit cell in the structures with $Li^+$ concentration. Also, the parameters are changed mobile ion valency and size [10]. For example, the repulsion between same charge ions is increased with increasing ion size and form larger bottleneck size and interstitial. In the case of the ion valency effect, ionic conductivity decreases with increasing valency because the electrostatic interaction between mobile ion and opposite charge ions is increased and decrease the ion diffusion.

## 1-3. Inorganic/ceramic electrolyte

### 1-3-1. Oxide solid electrolyte

Most oxide-based solid electrolytes produced have focused on using NASICON, perovskite, garnet, and LISICON structures. The NASICON structures such as $Li_{1.3}Al_{0.3}Ti_{1.7}(PO_4)_3$ have high electrochemical oxidative voltage window (~6V versus $Li^+/Li$) [22] as well as stability from air and moisture. The perovskite such as $Li_3La_{(2/3)-x}d_{(1/3)-2x}TiO_3$ (LLTO, $0 < x < 0.16$), is representative material due to tis high ionic conductivity at room temperature ($10^{-3}$ S/cm). In the case of the garnet structure, the grain boundaries can go through dendrite and have large interfacial resistance due to their being no wet surface next to the Li metal [23]. The LISICON structures such as $Li_{3x}La_{2/3-x}TiO_3$ and $Li_{3/8}Sr_{7/16}Zr_{1/4}Ta_{3/4}O_3$, have low contact with Li metal due to the reduction of Ti and Ta ions [23].

#### 1-3-1-1. NASICON

NASICON-like structures are generally known as a rhombohedral unit cell and $R\bar{3}c$ with a few monoclinic and orthorhombic phases [24]. Representatively, $L_{1+6x}M_{4+2-x}M'_{3+x}(PO_4)_3$ phosphates (L = Li or Na and M =Ti, Ge, Sn, Hf, or Zr and M′ = Cr, Al, Ga, Sc, Y, In, or La) are composed with $MO_6$ octahedra connected by corner sharing with $PO_4$ tetrahedral to form 3D interconnected channels and two types of interstitial positions where mobile cations are distributed in Figure. 1.7 [25]. The M1 sites which are 6-fold coordination located between two $MO_6$ octahedral while M2 sites that are 8-fold coordinated and located between two columns of $MO_6$ octahedral [26]. The lithium ions diffuse from on site to another through bottlenecks.

NASICON-like materials $LiA_2^{IV}(PO_4)_3$ showed ionic conductivity $10^{-5}$ S/cm at room temperature in 2009 [27]. To solve size mismatch between $Li^+$ and $TiO_6$ octahedral, a few materials have been developed and exhibited improved ionic conductivity such as the

$Li_{1.3}Al_{0.3}Ti_{1.7}(PO_4)_3$ ($10^{-3}$ S/cm) [28]. Also, the materials have high electrochemical oxidative voltage window (~6V versus $Li^+/Li$) [22] as well as stability from air and moisture. However, the NASICON electrolytes containing Ti are unstable with Li metal at low potentials.

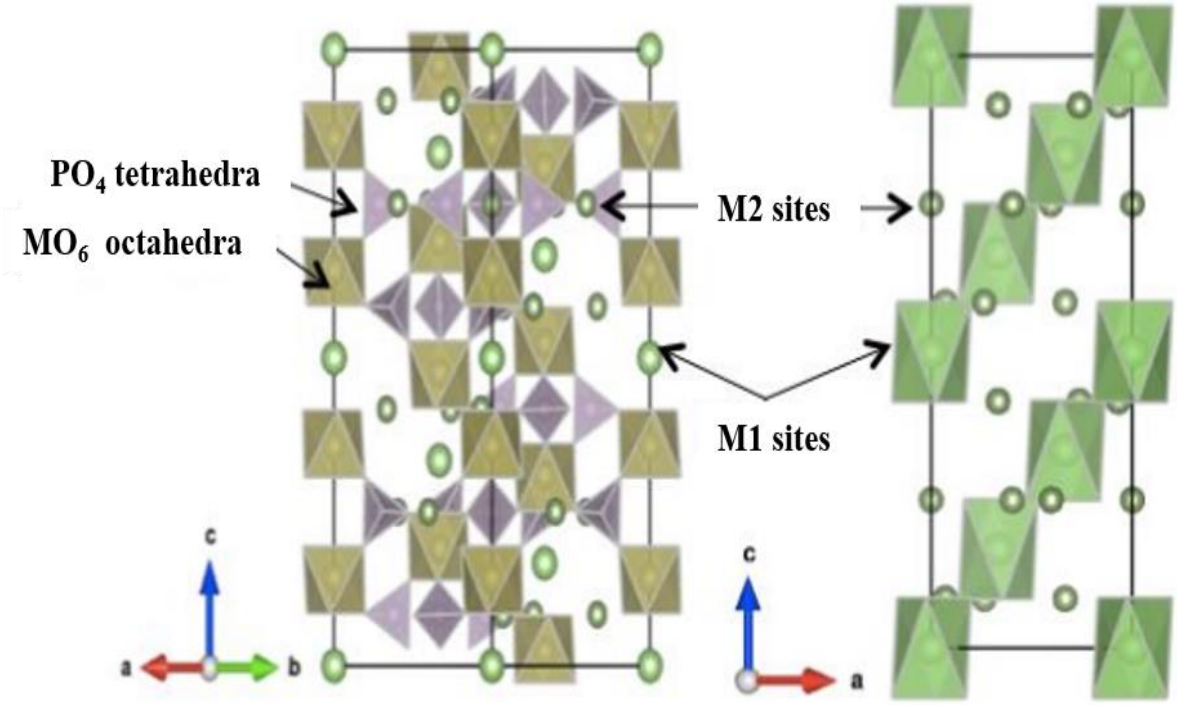


**Figure 1.7** Schematic structure of NASICON-like [25].

### 1-3-1-2. Perovskite

Perovskite materials having chemical formula $ABO_3$ is well known as the representative cubic phase with space group $Pm\bar{3}m$. Among the structural materials, lithium-lanthanum-titanates, $Li_3La_{(2/3)-x}d_{(1/3)-2x}TiO_3$ (LLTO, $0 < x < 0.16$), is representative material due to tis high ionic conductivity at room temperature ($10^{-3}$ S/cm) [15]. The crystal structure of LLTO is in Figure 1.8 [27]. The A site cations, which were $Li^+$ and $La^{3+}$ in the cubic α-phase, were randomly distributed, while the A sites of the ordered β-LLTO had a doubled poerovskite stuructre, with an alternating arrangement of $La^+$ rich and Li vacancy rich layers along the c axis [28]. Not only high ionic conductivity, the materials have many advantages such as stability in air and moisture, wide stability temperature window (to 1600K), good electrochemical stability (>8V). However, the materials have not been applied to commercial solid battery system because of its unsuitable for use with lithium and graphite negative electrodes [7, 15], high temperature sintering for synthesis, lower ionic conductivity than that of single crystal due blocking grain boundaries [22, 29].

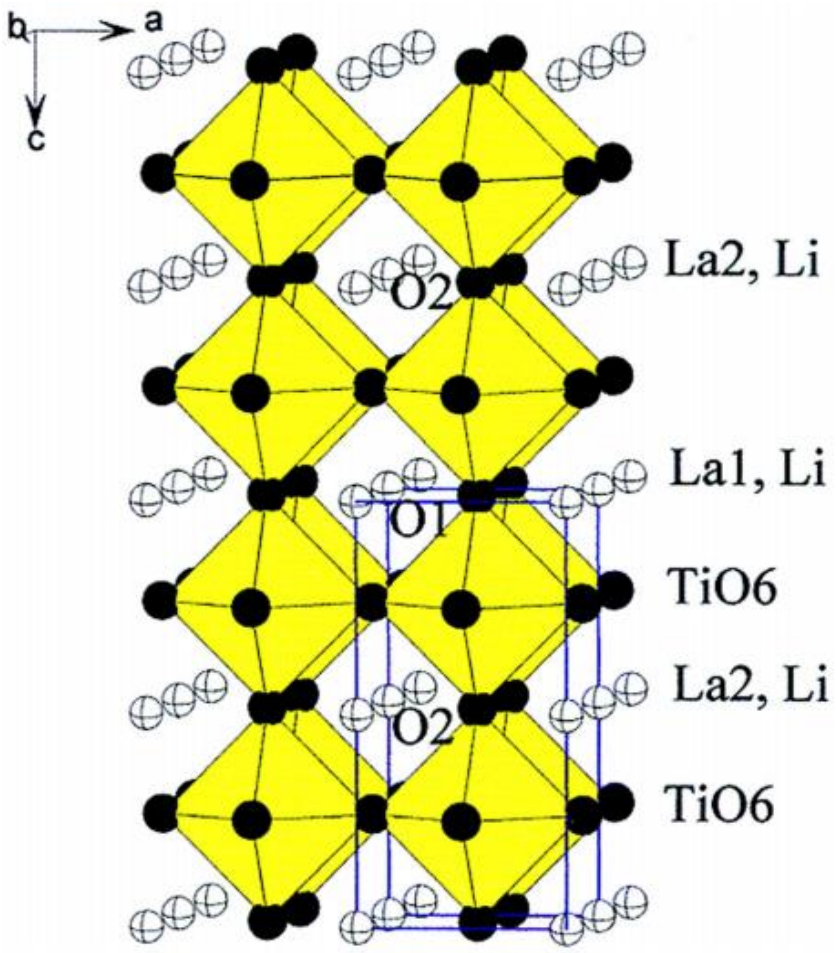


**Figure 1.8** Schematic structure of perovskite-type LLTO [27].

### 1-3-1-3. Garnet

The garnets exhibit a general chemical formula of $A_3B_2(XO_4)_3$ (A = Ca, Mg, Y, La or rare earth; B = Al, Fe, Ga, Ge, Mn, Ni or X = Si, Ge, Al) where A, B and C are eight, six and four oxygen coordinated cation sites, which crystalize in a face centered cubic structure with the space group $Ia\bar{3}d$ (Figure 1.9) [30]. Because the garnet electrolytes high $Li^+$ concentration 5~7 Li atoms per formula unit and can accommodate excess $Li^+$ at octahedral sites than that of number of lithium at the tetrahedral sites [30], the ionic conductivity of the electrolytes can be controlled by increasing Li concentration. For example, $Li_5La_3M_2O_{12}$ have low ionic conductivity of $10^{-6}$ S/cm at room temperature. However, the low conductivity can be improved when La and M sites are substituted with cations of higher or lower oxidation state than $La^{3+}$ and $M^{5+}$ with controlling the content of substitution elements such as $Li_{6.6}La_3Zr_{1.6}Sb_{0.4}O_{12}$ ($7.7x10^{-4}$ S/cm) and $Li_{6.2}La_3Zr_{1.2}Sb_{0.8}O_{12}$ ($4.5x10^{-4}$ S/cm) [31, 32]. Also, ionic conductivity of the garnet electrolytes can be improved by controlling shape control. For example, the particle shape of $Li_7La_3Zr_2O_{12}$ changes by contents of substitution element (Ga), and can be more dense pellets with same pressure [33]. As the results, the interface resistance by grain boundary was reduced. Although garnet electrolytes have high lithium concentration and ionic conductivity, the materials couldn`t be commercialized because of their unstable reactivity with cathode materials at the positive voltage window [34].

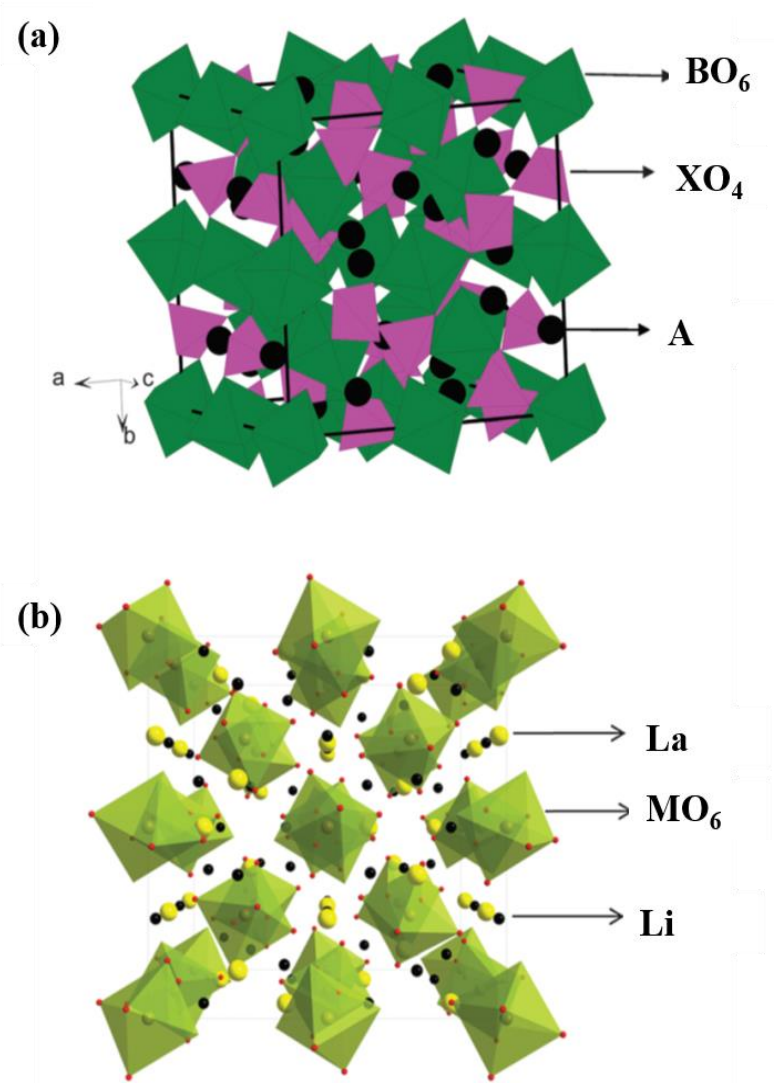


**Figure 1.9** Schematic structure of (a) garnet and (b) garnet-related $Li_5La_3M_2O_{12}$. [30].

## 1-3-1-4. LISICON

The crystal structure of LISICON-like compounds is related to the γ-$Li_3PO_4$ structure with orthorhombic unit cell and *pnma* space group, where all cations are tetrahedrally coordinated in Figure 1.10 [15, 35, 36]. The oxide LISICON-like materials such as $Li_{14}ZnGe_4O_{16}$ showed low ionic conductivity (~$10^{-7}$ S/cm) at room temperature by trapping of the mobile $Li^+$ ions by the immobile sub lattice at lower temperatures via the formation of defect complexes [27]. Recently, the thio-LISICON changed $O^{2-}$ to $S^{2-}$ have been studied for high lithium ion conductivity by 3 orders of magnitude at room temperature [15]. Many thio materials such as $Li_{10}MP_2S_{12}$ (M=Si,Ge, and Sn), $Li_{11}Si_2PS_{12}$ showed high ionic conductivity [14, 37, 38]. Especially, $Li_{10}GeP_2S_{12}$ showed highest lithium ion conductivity (~$10^{-2}$ S/cm) at 27℃ [38] among current ceramic electrolytes [15]. As the radius of $S^{2-}$ is higher than $O^{2-}$, this substitution can significantly enlarge the size of $Li^+$ transport bottlenecks. Also, $S^{2-}$ has better polarization capability than $O^{2-}$. Consequently, the the interaction between skeleton and $Li^+$ ions is weaker and make the mobility of $Li^+$ [39]. The thio-LISICON materials also have favorable advantage, which is reduction of grain boundary resistance by simple cold-press of electrolytes powders because of its good ductility compare with hard oxide materials [27].

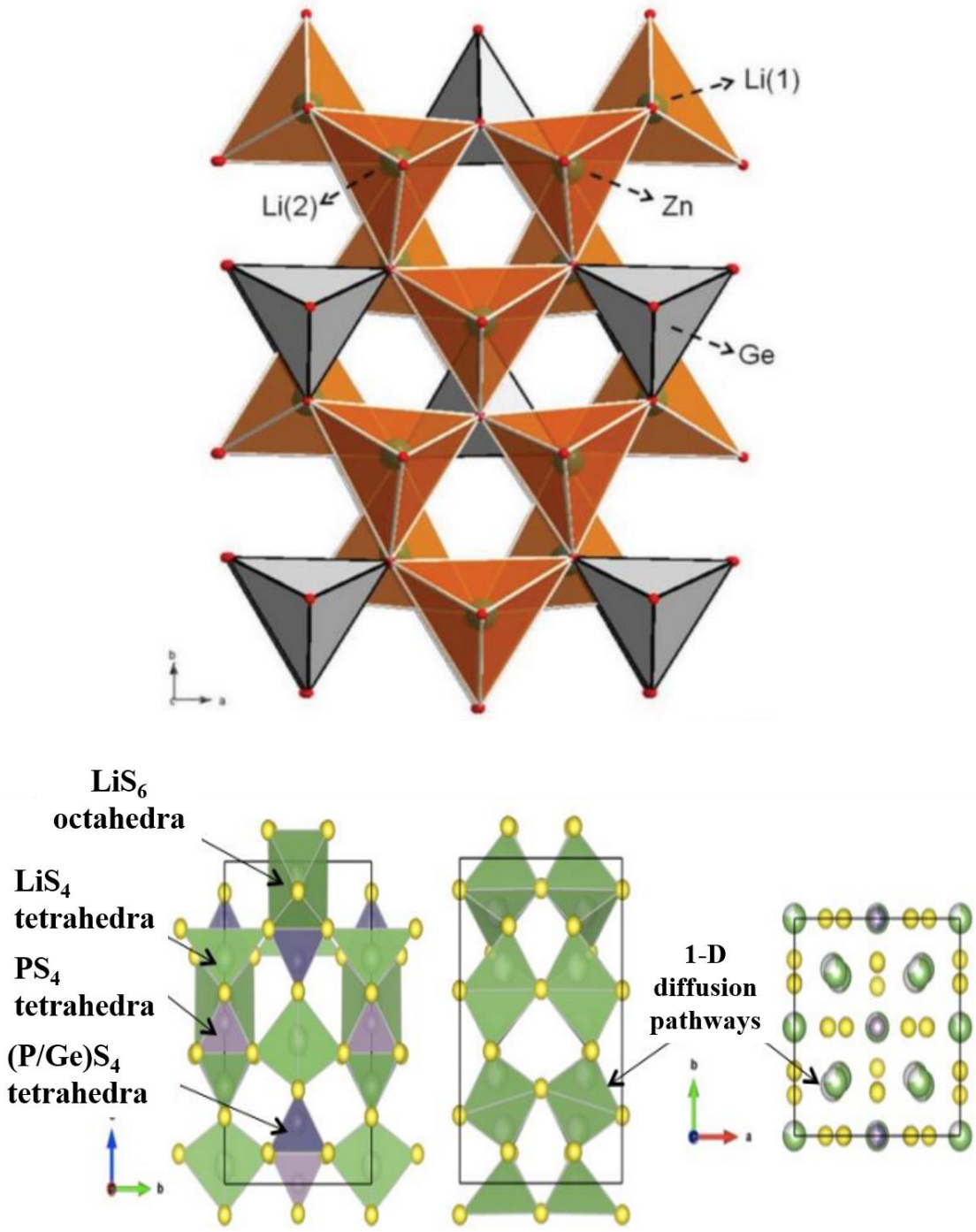


**Figure 1.10** Schematic structure of LISICON-like [36].

## 1-3-2. Sulfide solid electrolyte

Sulfide-based solid electrolytes have a smaller grain boundary and higher ionic conductivity compared with oxide-based electrolytes due to the high polarizability of sulfur ions and their low binding force with lithium ions [40, 41]. Even the ionic migration of $S^{2-}$ is larger than that of $O^{2-}$ due to the large ionic radius of $S^{2-}$ compared to $O^2$ [42].

### 1-3-2-1. Thio-LISICON

The thio-LISICON materials such as $Li_{3.25}Ge_{0.25}P_{0.75}S_4$ and $Li_{10}GeP_2S_{12}$ were known that the materials have theoretical wide electrochemical stability window from 0V to 4V versus $Li/Li^+$ [43]. However, many results have been explained that the sulfide materials have narrow electrochemical window and react with cathode and anode [27, 37, 44, 45]. Because of the larger size and smaller electronegativity of $S^{2-}$ than $O^{2-}$, the chemical interaction in the crystals structure of thio materials is week. As the results, the materials composed with $S^{2-}$ anion have similar stability of less than 25meV per atom and show unstable characteristic than oxide materials. The results is coincide with bandgaps calculation: O substituted LMPO materials have a larger bandgap than the LMPS materials [45]. Actually, almost thio materials react and are decomposed with cathode materials and anode materials including Li metal [45, 46]. In addition, the materials are difficult to synthesis at general atmosphere because they are very sensitive to air and moisture.

### 1-3-2-2. Argyrodite

Argyrodites form a class of chalcogenide structures related to the mineral $Ag_8GeS_6$, which includes various fast $Ag^+$ or $Cu^+$ ion conductors such as $A_7PS_5X$ ($A=Ag^+$, $Cu^+$). Recently, Deiseroth et al. [47] could synthesize the analogue cubic $Li^+$ argyrodytes with formula $Li_6PS_5X$ (X=Cl, Br, I) and $Li_7PS_6$ [44, 48]. The structure similar to $Ag_8GeS_6$ because the atomic radius of silver ions is similar with lithium ions and it has the same coordination number, the structure in which anions in the Argyrodyte structure are substituted with lithium ions. $Li_6PS_5Br$ showed the highest Li-ion mobility among $Li_6PS_5X$ (X = Cl, Br, I), as indicated by Nuclear Magnetic Resonance (NMR) and also the ionic conductivity value [49].

## 1-3-3. Hydride solid electrolyte

Complex hydrides are expressed by the general formula M(M′Hn), where M is the metal cation and M′Hn is the complex anion (e.g., $[BH_4]^-$, $[NH_2]^-$, $[AlH_4]^-$). Matsuo et al. [50] developed a new category of Solid-state lithium fast-ion conductor using a complex hydride. Ionic conductivity of $LiBH_4$ at low temperature in the range of $10^{-8}$ -$10^{-6}$ S $cm^{-1}$ and it high temperature shows high conductivity reach up to $10^{-3}$ S $cm^{-1}$. However, hydride-based solid electrolytes cause side reactions at the interface when they are in contact with an anode, which is an oxide, to produce the following materials to increase resistance and decrease capacity.

## 1-4. Introduction of lithium aluminum titanium phosphate

### 1-4-1. Crystal structure of lithium aluminum titanium phosphate

Solid electrolytes based $LiTi_2(PO_4)_3$ have been studied because of their high lithium conductivity. It has been reported that the conductivity for $LiTi_2(PO_4)_3$ increases appreciably of $Ti^{4+}$ in the phosphate is partially substituted by a larger cation. Unlike perovskite-type and garnet-type oxides, NASICON type structure is pretty stable in an aqueous environment. Lithium Aluminum Titanium Phosphate (LATP) is kind of phosphate-based electrolyte from NASICON-like solid electrolyte. $Li_{1+x}Al_xTi_{2-x}(PO_4)_3$, is mainly composed of $LiTi_2(PO_4)_3$ with NASICON type structure, among which $Ti^{4+}$ ions are partly replaced by $Al^{3+}$ ions. $LiTi_2(PO4)_3$ is composed of $TiO_6$ octahedron and $PO_4$ tetrahedron, which are connected by their angles to form a three-dimensional (3D) network structure as shown in Figure 1.11. This connection causes cavities where Li-ions reside, and bottlenecks in which Li-ions pass through. There are three different Li sites (Li(1), Li(2) Li(3)) in $LiTi_2(PO_4)_3$ structure, Li(1) is expected to be fully occupied while Li partially fills Li(2) and Li(3) sites. In $LiTi_2(PO_4)_3$ $TiO_6$ octahedron and $PO_4$ tetrahedron form a rhombohedral unit cell. Partial replacement of $Ti^{4+}$ with a smaller $Al^{3+}$ ion reduces the unit cell dimension, leading to the densifying effect and ionic conductivity enhancement [51].

Instead of LATP, there are several phosphate-based electrolytes such as Lithium Aluminum Germanium Phosphate, and Lithium Aluminum Zirconium Phosphate. LATP has the advantage that it has a relatively high ionic conductivity although it is still lower when compared to germanium-based phosphate, but relatively higher when compared to zirconium-based phosphate (LAGP> LATP> LAZP). However, LATP has a lower production cost compared to LAGP which can be developed for low-cost solid electrolyte materials [52]. LATP particle size affects the energy capacity and efficiency of the ion conductivity in LATP, this is due to the

larger surface area which causes the diffusion of lithium ions to be higher [54]. LATP is a ceramic material which has the advantage of being more stable in extreme conditions, non-toxic, and environmentally friendly compared to other materials for large-scale applications. LATP synthesis can be carried out by various methods including solid-state, melt-quenching, spark plasma sintering (SPS), microwave assister sintering, sol-gel, co-precipitation, hydrothermal, spray-drying, and so on [51, 53].

Figure. 1.12 presents the total conductivity results with x in the $Li_{1+x}M_xTi_{2-x}(PO_4)_3$ (Where M=Al, Cr, Ga, Fe, Sc, In, Lu, Y, La) systems at 298 K. The conductivity for the pellets of $LiTi_2(PO_4)_3$ (x=0) was as low as $2x10^{-6}$ S $cm^{-1}$ and greatly increased by the $M^{3+}$ substitution having a maximum value at around x=0.3 for all the systems examined except for the $Cr^{3+}$ system. The maximum conductivity was $7x10^{-4}$ S $cm^{-1}$ at 298 K for $Li_{1.3}M_{0.3}Ti_{1.7}(PO_4)_3$ (M=Al or SC) [54]. Figure 1.13 Shows calculated electrochemical stability ranges of various solid electrolyte materials grouped by anion, with corresponding binary for comparison [55]. As the results of the graph, materials with strongly bound polyanions such as the phosphate have much wider stability windows than sulfide materials. These results mean the tendency of increasing anodic stability with increasing electronegativity related with bond strength.

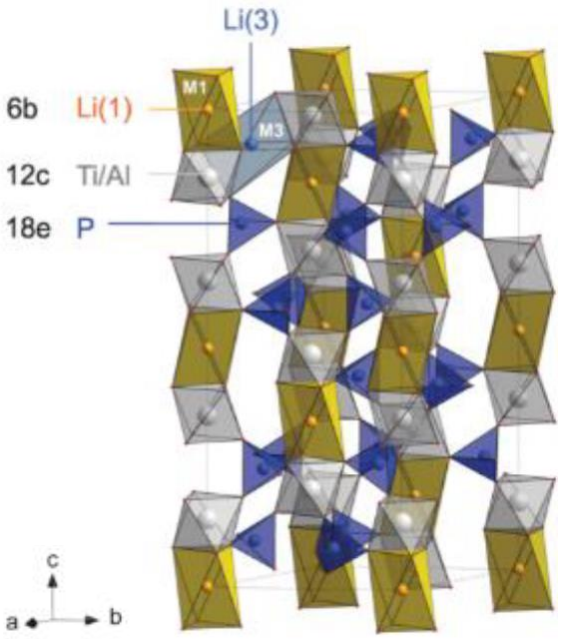


**Figure 1.11** Crystal structure for LATP solid electrolyte with rhombohedral lattice [51].

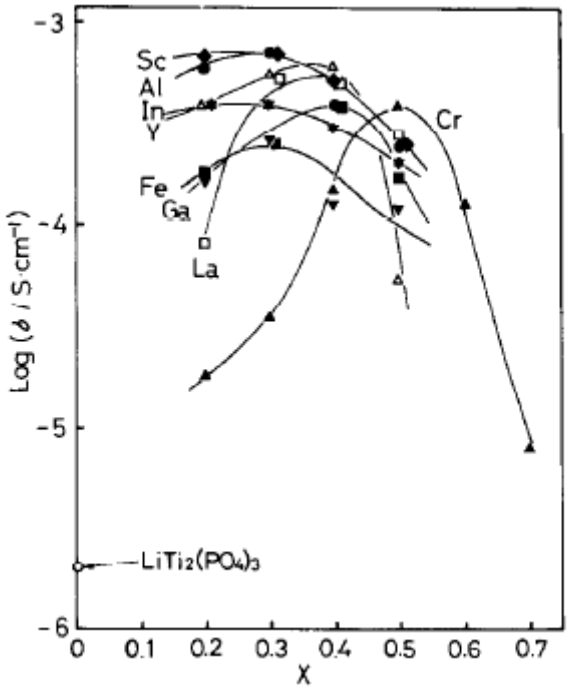


**Figure 1.12** The total conductivity versus x relation for the $Li_{1+x}M_xTi_{2-x}(PO_4)_3$ systems at 298K [54].

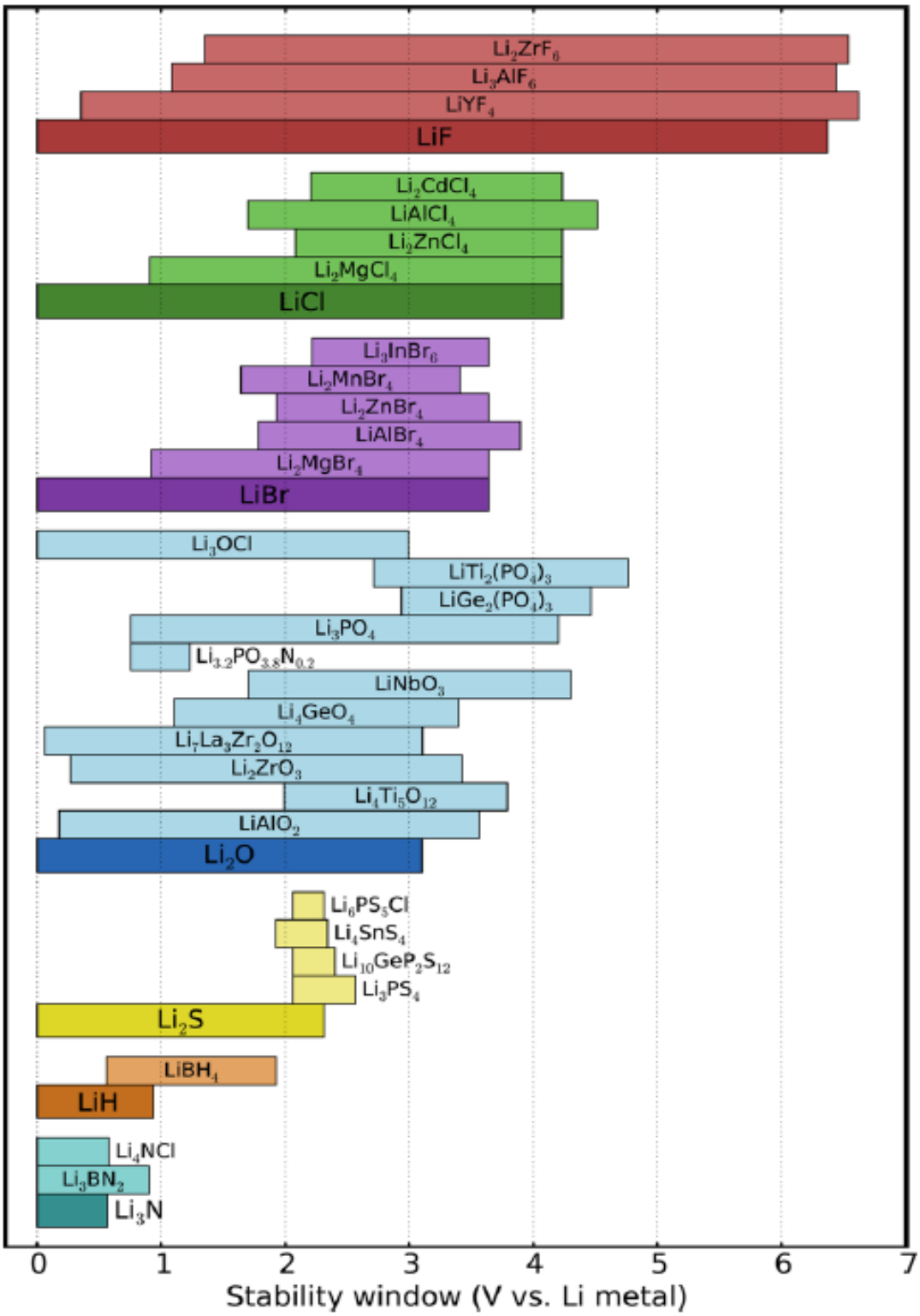


**Figure 1.13** Calculated electrochemical stability window of the solid electrolytes [55].

### 1-4-2. Strategy for increasing electrochemical performances of oxide electrolytes

NASICON-type oxide solid electrolyte have good water stability, they also show promise for next-generation aqueous Li batteries. Since the oxide solid electrolytes show a promising prospect in the future, there are several approach should be done for improve the performance of oxide solid electrolytes by decreasing or removing its drawbacks. NASICON-type solid electrolyte are expected to obtain further enhancement in several ways, such as: [51]

1. Increasing their conductivities to $10^{-3}$ S/cm.
2. Improving the interfacial stability of the electrolyte with a Li metal anode to reduce the interfacial resistance and prevent interfacial reactions.
3. Modification of the solid electrolyte contacts with cathode materials to increase ion mobility in cathode composites.
4. Searching for novel electrode materials that are stable enough to cycle without Li dendrite formation, but high performing enough to make the battery stable.

## 1-5. Purpose

Based on above previous studies, we investigated the LATP solid electrolyte with modified solid-state synthesis for all-solid-state lithium batteries. In this work, we aimed to investigate the effect of binder to the LATP solid electrolytes. Water-soluble binders such as PVA, CMC, and PAA were used to increase the ionic conductivity of solid electrolyte. In addition, to compare the effect of binder's addition to the solid electrolyte, we synthesized the binder-modified LATP solid electrolytes and silver-modified LATP with addition of numerous binder. Prior to experiments to improve the ionic conductivity and electrochemical stability, the basic studies for physical and electrochemical properties in this experiments were conducted and explained. The XRD and structural surface morphology analysis were measured for physical characterization and EIS, CV, and DC-cycling were measured for electrochemical analysis for both LATP and silver-modified LATP.

# References


[1] Jung-Ki Park, *Principles and Applications of Lithium Secondary Batteries*. John Wiley & Sons, 2012.

[2] J.-M. Tarascon and M. Armand, "Issues and challenges facing rechargeable lithium batteries," *Nature*, pp. 359–367, 2001.

[3] J. W. Fergus, "Recent developments in cathode materials for lithium ion batteries," *J. Power Sources*, vol. 195, no. 4, pp. 939–954, 2010.

[4] C. M. Julien, A. Mauger, K. Zaghib, and H. Groult, "Comparative issues of cathode materials for Li-ion batteries," *Inorganics*, vol. 2, no. 1, pp. 132–154, 2014.

[5] D. Deng, "Li-ion batteries: Basics, progress, and challenges," *Energy Sci. Eng.*, vol. 3, no. 5, pp. 385–418, 2015.

[6] H. Lee, M. Yanilmaz, O. Toprakci, K. Fu, and X. Zhang, "A review of recent developments in membrane separators for rechargeable lithium-ion batteries," *Energy Environ. Sci.*, vol. 7, no. 12, pp. 3857–3886, 2014.

[7] A. Manuel Stephan and K. S. Nahm, "Review on composite polymer electrolytes for lithium batteries," *Polymer (Guildf).*, vol. 47, no. 16, pp. 5952–5964, 2006.

[8] N. Q. Minh, "Ceramic Fuel Cells," *J. Am. Ceram. Soc.*, vol. 76, no. 3, pp. 563–588, 1993.

[9] J. B. Goodenough and Y. Kim, "Challenges for rechargeable Li batteries," *Chem. Mater.*, vol. 22, no. 3, pp. 587–603, 2010.

[10] K. Xu, "Nonaqueous liquid electrolytes for lithium-based rechargeable batteries," *Chem. Rev.*, vol. 104, no. 10, pp. 4303–4417, 2004.

[11] Y. Seino, T. Ota, K. Takada, A. Hayashi, and M. Tatsumisago, "A sulphide lithium super ion conductor is superior to liquid ion conductors for use in rechargeable batteries," *Energy Environ. Sci.*, vol. 7, no. 2, pp. 627–631, 2014.

[12] J. Zhang, R. Gao, L. Sun, H. Zhang, Z. Hu, and X. Liu, "Unraveling the multiple effects of $Li_2ZrO_3$ coating on the structural and electrochemical performances of $LiCoO_2$ as high-voltage cathode materials," *Electrochim. Acta*, vol. 209, pp. 102–110, 2016.

[13] S. Wenzel, D. A. Weber, T. Leichtweiss, M. R. Busche, J. Sann, and J. Janek, "Interphase

formation and degradation of charge transfer kinetics between a lithium metal anode and highly crystalline $Li_7P_3S_{11}$ solid electrolyte," *Solid State Ionics*, vol. 286, pp. 24–33, 2016.

[14] N. Kamaya *et al.*, "A lithium superionic conductor," *Nat. Mater.*, vol. 10, no. 9, pp. 682–686, 2011.

[15] J. C. Bachman *et al.*, "Inorganic Solid-State Electrolytes for Lithium Batteries: Mechanisms and Properties Governing Ion Conduction," *Chem. Rev.*, vol. 116, no. 1, pp. 140–162, 2016.

[16] and B. S. Dyer, Chris K., Patrick T. Moseley, Zempachi Ogumi, David AJ Rand, *Encyclopedia of Electrochemical Power Sources*. Elsevier Science & Technology, 2013.

[17] Y. C. Jung *et al.*, "Ceramic separators based on $Li^+$-conducting inorganic electrolyte for high-performance lithium-ion batteries with enhanced safety," *J. Power Sources*, vol. 293, pp. 675–683, 2015.

[18] A. Martínez-Juárez, C. Pecharromán, J. E. Iglesias, and J. M. Rojo, "Relationship between activation energy and bottleneck size for $Li^+$ ion conduction in NASICON materials of composition $LiMM'(PO_4)_3$; M, M′ = Ge, Ti, Sn, Hf," *J. Phys. Chem. B*, vol. 102, no. 2, pp. 372–375, 1998.

[19] A. R. Rodger, J. Kuwano, and A. R. West, "$Li^+$ ion conducting γ solid solutions in the systems $Li_4XO_4$-$Li_3YO_4$: X=Si, Ge, Ti; Y=P, As, V; $Li_4XO_4$-$LiZO_2$: Z=Al, Ga, Cr and $Li_4GeO_4$-$Li_2CaGeO_4$," *Solid State Ionics*, vol. 15, no. 3, pp. 185–198, 1985.

[20] J. B. Goodenough, "Oxide-ion electrolytes," *Annu. Rev. Mater. Res.*, vol. 33, pp. 91–128, 2003.

[21] R. Tarneberg and A. Lund, "Ion diffusion in the high-temperature phases $Li_2SO_4$, $LiNaSO_4$, $LiAgSO_4$ and $Li_4Zn(SO_4)_3$," *Solid State Ionics*, vol. 90, no. 1–4, pp. 209–220, 1996.

[22] P. Knauth, "Inorganic solid Li ion conductors: An overview," *Solid State Ionics*, vol. 180, no. 14–16, pp. 911–916, 2009.

[23] Y. Li *et al.*, "Fluorine-Doped Antiperovskite Electrolyte for All-Solid-State Lithium-Ion Batteries," *Angew. Chemie*, vol. 128, no. 34, pp. 10119–10122, 2016.

[24] H. Aono, E. Sugimoto, Y. Sadaoka, N. Imanaka, and G. Adachi, "The Electrical Properties of Ceramic Electrolytes for $LiM_xTi_{2-x}(PO_4)_3 + yLi_2O$, M = Ge , Sn , Hf , and Zr Systems," *J. Electrochem. Soc.*, vol. 140, no. 7, pp. 1827–1833, 1993.

[25] G. F. Ortiz, M. C. López, P. Lavela, C. Vidal-Abarca, and J. L. Tirado, "Improved lithium-ion transport in NASICON-type lithium titanium phosphate by calcium and iron doping," *Solid State Ionics*, vol. 262, pp. 573–577, 2014.

[26] R. Norhaniza, R. H. Y. Subban, and N. S. Mohamed, "Cr and V substituted $LiSn_2P_3O_{12}$ solid electrolyte materials," *J. Power Sources*, vol. 244, pp. 300–305, 2013.

[27] C. Cao, Z. Bin Li, X. L. Wang, X. B. Zhao, and W. Q. Han, "Recent advances in inorganic solid electrolytes for lithium batteries," *Front. Energy Res.*, vol. 2, no. JUN, pp. 1–10, 2014.

[28] P. Hartmann *et al.*, "Degradation of NASICON-type materials in contact with lithium metal: Formation of mixed conducting interphases (MCI) on solid electrolytes," *J. Phys. Chem. C*, vol. 117, no. 41, pp. 21064–21074, 2013.

[29] S. Wenzel, T. Leichtweiss, D. Krüger, J. Sann, and J. Janek, "Interphase formation on lithium solid electrolytes - An in situ approach to study interfacial reactions by photoelectron spectroscopy," *Solid State Ionics*, vol. 278, pp. 98–105, 2015.

[30] V. Thangadurai, S. Narayanan, and D. Pinzaru, "Garnet-type solid-state fast Li ion conductors for Li batteries: Critical review," *Chem. Soc. Rev.*, vol. 43, no. 13, pp. 4714–4727, 2014.

[31] E. J. Cussen, "Structure and ionic conductivity in lithium garnets," *J. Mater. Chem.*, vol. 20, no. 25, pp. 5167–5173, 2010.

[32] S. Ramakumar, L. Satyanarayana, S. V. Manorama, and R. Murugan, "Structure and $Li^+$ dynamics of Sb-doped $Li_7La_3Zr_2O_{12}$ fast lithium ion conductors," *Phys. Chem. Chem. Phys.*, vol. 15, no. 27, pp. 11327–11338, 2013.

[33] H. El Shinawi and J. Janek, "Stabilization of cubic lithium-stuffed garnets of the type '$Li_7La_3Zr_2O_{12}$' by addition of gallium," *J. Power Sources*, vol. 225, pp. 13–19, 2013.

[34] K. H. Kim *et al.*, "Characterization of the interface between $LiCoO_2$ and $Li_7La_3Zr_2O_{12}$ in an all-solid-state rechargeable lithium battery," *J. Power Sources*, vol. 196, no. 2, pp.

764–767, 2011.

[35] A. R. West, “Crystal chemistry of some tetrahedral oxides,” *Zeitschrift fur Krist. - New Cryst. Struct.*, vol. 141, no. 5–6, pp. 422–436, 1975.

[36] J. Lau, R. H. DeBlock, D. M. Butts, D. S. Ashby, C. S. Choi, and B. S. Dunn, “Sulfide Solid Electrolytes for Lithium Battery Applications,” *Adv. Energy Mater.*, vol. 8, no. 27, pp. 1–24, 2018.

[37] A. Kuhn, O. Gerbig, C. Zhu, F. Falkenberg, J. Maier, and B. V. Lotsch, “A new ultrafast superionic Li-conductor: Ion dynamics in $Li_{11}Si_2PS_{12}$ and comparison with other tetragonal LGPS-type electrolytes,” *Phys. Chem. Chem. Phys.*, vol. 16, no. 28, pp. 14669–14674, 2014.

[38] P. Bron, S. Johansson, K. Zick, J. S. A. Der Günne, S. Dehnen, and B. Roling, “$Li_{10}SnP_2S_{12}$: An affordable lithium superionic conductor,” *J. Am. Chem. Soc.*, vol. 135, no. 42, pp. 15694–15697, 2013.

[39] M. Murayama *et al.*, “Synthesis of new lithium ionic conductor thio-LISICON - Lithium silicon sulfides system,” *J. Solid State Chem.*, vol. 168, no. 1, pp. 140–148, 2002.

[40] H. Muramatsu, A. Hayashi, T. Ohtomo, S. Hama, and M. Tatsumisago, “Structural change of $Li_2S$-$P_2S_5$ sulfide solid electrolytes in the atmosphere,” *Solid State Ionics*, vol. 182, no. 1, pp. 116–119, 2011.

[41] T. Ohtomo, A. Hayashi, M. Tatsumisago, and K. Kawamoto, “Suppression of $H_2S$ gas generation from the $75Li_2S$-$25P_2S_5$ glass electrolyte by additives,” *J. Mater. Sci.*, vol. 48, no. 11, pp. 4137–4142, 2013.

[42] M. Tatsumisago and A. Hayashi, “Sulfide Glass-Ceramic Electrolytes for All-Solid-State Lithium and Sodium Batteries,” *Int. J. Appl. Glas. Sci.*, vol. 5, no. 3, pp. 226–235, 2014.

[43] R. Kanno and M. Murayama, “Lithium Ionic Conductor Thio-LISICON: The $Li_2S$-$GeS_2$-$P_2S_5$ System,” *J. Electrochem. Soc.*, vol. 148, no. 7, p. A742, 2001.

[44] R. P. Rao and S. Adams, “Studies of lithium argyrodite solid electrolytes for all-solid-state batteries,” *Phys. Status Solidi Appl. Mater. Sci.*, vol. 208, no. 8, pp. 1804–1807, 2011.

[45] Y. Mo, S. P. Ong, and G. Ceder, "First principles study of the $Li_{10}GeP_2S_{12}$ lithium super ionic conductor material," *Chem. Mater.*, vol. 24, no. 1, pp. 15–17, 2012.

[46] H. Chung and B. Kang, "Increase in grain boundary ionic conductivity of $Li_{1.5}Al_{0.5}Ge_{1.5}(PO_4)_3$ by adding excess lithium," *Solid State Ionics*, vol. 263, pp. 125–130, 2014.

[47] H.-J. Deiseroth *et al.*, "$Li_6PS_5X$: A Class of Crystalline Li-Rich Solids With an Unusually High $Li^+$ Mobility," *Angew. Chemie*, vol. 120, no. 4, pp. 767–770, 2008.

[48] R. B. Beeken, J. J. Garbe, J. M. Gillis, N. R. Petersen, B. W. Podoll, and M. R. Stoneman, "Electrical conductivities of the $Ag_6PS_5X$ and the $Cu_6PSe_5X$ (X=Br, I) argyrodites," *J. Phys. Chem. Solids*, vol. 66, no. 5, pp. 882–886, 2005.

[49] E. Rangasamy *et al.*, "An iodide-based $Li_7P_2S_8I$ superionic conductor," *J. Am. Chem. Soc.*, vol. 137, no. 4, pp. 1384–1387, 2015.

[50] M. Matsuo, H. Oguchi, H. Maekawa, H. Takamura, S. Orimo, and M. M. Volume, "Complex Hydrides : A New Category of Solid-state Lithium Fast-ion Conductors," vol. 5, pp. 5–13, 2011.

[51] R. DeWees and H. Wang, "Synthesis and Properties of NaSICON-type LATP and LAGP Solid Electrolytes," *ChemSusChem*, vol. 12, no. 16, pp. 3713–3725, 2019.

[54] V. Thangadurai, A. K. Shukla, and J. Gopalakrishnan, "New lithium-ion conductors based on the NASICON structure," *J. Mater. Chem.*, vol. 9, no. 3, pp. 739–741, 1999.

[53] E. Zhao, F. Ma, Y. Jin, and K. Kanamura, "Pechini synthesis of high ionic conductivity $Li_{1.3}Al_{0.3}Ti_{1.7}(PO_4)_3$ solid electrolytes: The effect of dispersant," *J. Alloys Compd.*, vol. 680, pp. 646–653, 2016.

[54] H. Aono, E. Sugimoto, Y. Sadaoka, N. Imanaka, and G. ya Adachi, "Ionic conductivity and sinterability of lithium titanium phosphate system," *Solid State Ionics*, vol. 40–41, no. PART 1, pp. 38–42, 1990.

[55] W. D. Richards, L. J. Miara, Y. Wang, J. C. Kim, and G. Ceder, "Interface Stability in Solid-State Batteries," *Chem. Mater.*, vol. 28, no. 1, pp. 266–273, 2016.

# Chapter 2. General Experiments

## 2-1. Physical characterization

### 2-1-1. X-ray diffraction (XRD)

X-ray powder diffraction (XRD) is essential technique that uses the diffraction of X-rays on powder or microcrystalline samples for the study of crystal structures and those of volume. The most popular analysis method for structural changes by crystal structures and environments (atmosphere, temperature etc.) of the powder samples. It is based on constructive interference of monochromatic X-ray and a crystalline sample. Therefore, it is possible to Figure out the shape of crystalline from the diffraction of a crystal in any direction, the structure of material is also contained in the forward scattering. The inorganic powders were usually used as the sample for the diffraction analysis. The samples were interacted with the incident X-ray beam as followed Bragg`s Law equation (Figure 2.1).

$$n\lambda = 2d_{hkl}\sin\theta_{hkl} \text{ (Bragg equation)} \quad (n=1, 2, 3 \ldots) \qquad (2.1)$$

Where λ is frequency of incident beam, d is d-spacing, θ is the diffraction angles when the samples interact with incident beam, hkl is miller index. This law related the wavelength of electromagnetic radiation to the diffraction angle and the lattice spacing in a crystalline powder. The difference of path length between reflections on neighboring planes is $d_{hkl}sin\theta_{hkl}$. For example, the smaller the distance d-spacing, the larger the diffraction angle $\theta$. When the wavelength λ increase, the diffraction angle $\theta$ increase. Because the difference of path length means the different interference between the diffraction wavelengths, the angle is main scale for determining the crystals. From the equations, the d-spacing can be calculated by considering Miller indices and unit cell parameter it was related 7 types of crystal system. Table 2.1 shows the crystal system and d-spacing [1 - 4]. The crystals depend on three cell parameters (a, b, c) and three angles ($\alpha, \beta, \gamma$). The crystals are different symmetries from the cubic crystal

composed with three same parameter values and three 90 degrees angles to triclinic. According to the rotational symmetry, there are 14 different Bravais Lattices in which similar points can be arranged in a three-dimensional space not 28 cases by French crystallographer August Bravais in 1848. The 14 Bravais Lattices are combined with 32-point group symmetries and finally, give the 230 space groups. This powerful analysis can be applied to almost inorganic materials which have quite electronic density except for low periodic number such as Li due to its low electronic density.

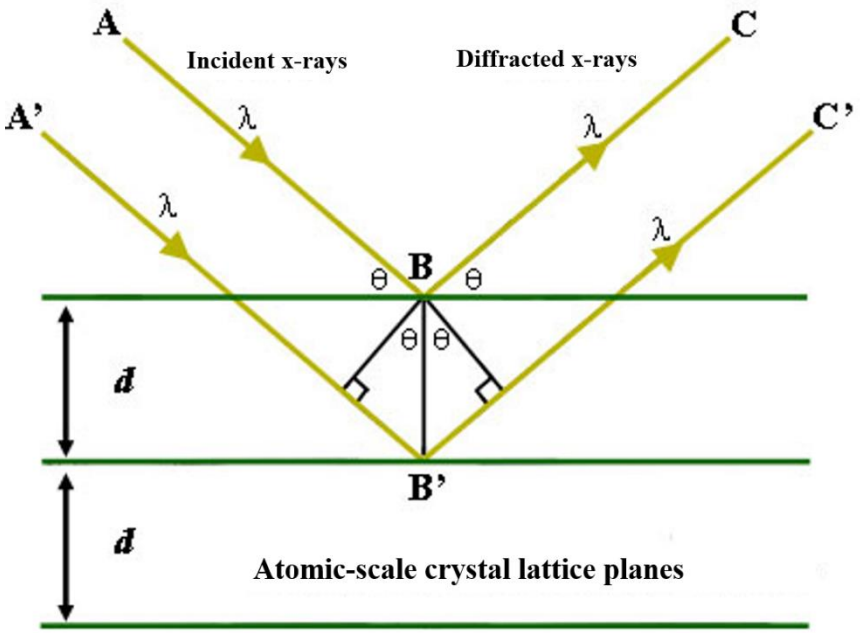


**Figure 2.1** Bragg reflection on a set of atomic planes.

**Table 2.1** Crystal system and Bravias lattice.

| Bravais lattice | Parameters | Simple (P) | Volume centered (I) | Base centered (C) | Face centered (F) |
|---|---|---|---|---|---|
| Triclinic | $a_1 \neq a_2 \neq a_3$<br>$\alpha_{12} \neq \alpha_{23} \neq \alpha_{31}$ | 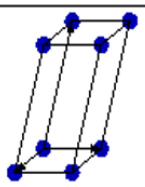 | | | |
| Monoclinic | $a_1 \neq a_2 \neq a_3$<br>$\alpha_{23} = \alpha_{31} = 90°$<br>$\alpha_{12} \neq 90°$ | 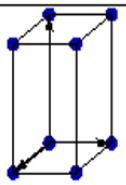 | 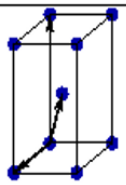 | | |
| Orthorhombic | $a_1 \neq a_2 \neq a_3$<br>$\alpha_{12} = \alpha_{23} = \alpha_{31} = 90°$ | 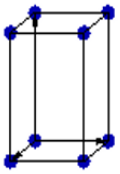 | 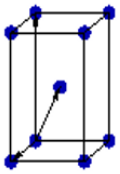 | 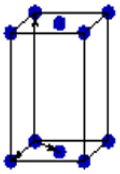 | 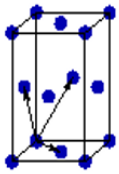 |
| Tetragonal | $a_1 = a_2 \neq a_3$<br>$\alpha_{12} = \alpha_{23} = \alpha_{31} = 90°$ | 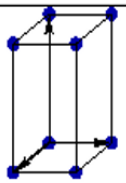 | 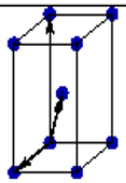 | | |
| Trigonal | $a_1 = a_2 = a_3$<br>$\alpha_{12} = \alpha_{23} = \alpha_{31} < 120°$ | 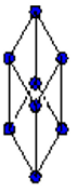 | | | |
| Cubic | $a_1 = a_2 = a_3$<br>$\alpha_{12} = \alpha_{23} = \alpha_{31} = 90°$ | 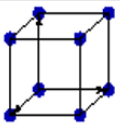 | 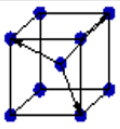 | | 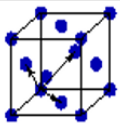 |
| Hexagonal | $a_1 = a_2 \neq a_3$<br>$\alpha_{12} = 120°$<br>$\alpha_{23} = \alpha_{31} = 90°$ | 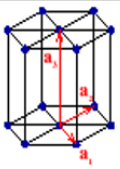 | | | |

## 2-1-2. Field emission scanning electron microscopy (FE-SEM)

FE-SEM is Field Emission Scanning Electron Microscope which operates with a high-energy electron beam in a scan pattern instead of light source. These electrons are released by a field emission source in a field emission gun. These electron emitters can produce up to 1000x the emission of a tungsten filament with high vacuum atmosphere to prevent unnecessary interaction between gas molecular and the electron beam. After the electrons beam exit the electron gun, monochromatic beam using metal apertures and magnetic lenses. And finally, the detectors of each type of electrons are placed in the microscopes that collect signals to produce an image of the patterns [5]. The electrons from the primary beam spread out in the sample to form the interaction volume. The size of the interaction volume depends on the accelerating voltage value of the primary electron beam and atomic number of the sample. The interaction volume increase with a larger accelerating voltage, but smaller for samples with a higher atomic number. Secondary electrons are produced from the surface of the sample or topmost part of the interaction volume and X-rays are generated within the whole of the interaction volume [6]. FE-SEM is used to visualize information of local area on the surface of chemicals. Also, the analysis can be combined with Energy dispersive X-ray spectroscopy (EDS) for good elemental analysis such as elemental composition near the surface of the samples with atomic number (Z)>3. The combination can also visualize the element distribution in a sample by mapping which showing the concentration of one element over a selected area of images of sample. SEM-EDS mapping analysis is an effective elemental mapping which showing how to concentrate one element varies over an area of images of material.

## 2-2. Electrochemical analysis

### 2-2-1. Electrochemical impedance spectroscopy (EIS)

Electrochemical impedance spectroscopy (EIS) is a powerful technique to measure the electrical impedance resistance of an electrode or whole cell system. The impedance of an electrochemical system is defined as the resistance when an AC voltage or current is applied over a range of frequencies. The current-voltage relationship of the impedance can be expressed as followed equation.

$$Z(w) = \frac{V(t)}{I(t)} = \frac{V_m sin(wt)}{I_m sin(wt-\theta)} = Zexp(j\theta) \quad (2.2)$$

Where v(t) and I(t) are AC voltage and current, Z(w) is impedance, w is frequency (w=2πf). The equation is derived by Euler`s rule as below:

$$\mathrm{Z(w)} = Z_{re} + iZ_{im} \quad (2.3)$$

Where $Z_{re}$ and $Z_{im}$ are the real and imaginary parts of the impedance in Nyquist plot which is one of the method for expressing impedance like Figure 2.2. From the obtained result, an equivalent circuit is deduced and is proved by the fitting procedure. The equivalent circuit gives the resistance component. For example, the real impedance value on x-axis from the O to initial value is mass transfer resistance considered as electrolyte resistance, the real value of the diameter of semicircle is charge transfer resistance related with a surface area of an electrode, and the Warburg region which is the tail is Warburg impedance related with lithium diffusion coefficient of an active material.

In the case of the solid electrolyte, the way to interpret the equivalent circuit is different. Fig 8 shows a suitable example for equivalent circuit of solid electrolyte. The real value from 0 to first semicircle means bulk resistance by a crystal structure and the insufficient contact between the particles of an active material and a solid electrolyte material. The second semicircle is the resistance by the grain boundary meaning a crack of solid electrolyte pellet. These factors are main resistance by solid electrolytes. The ionic conductivity of the solid electrolyte is calculated by below equation.

$$\sigma = \frac{\mathrm{l}}{\mathrm{RA}} = \mathrm{S/cm} \quad (2.4)$$

Where l is thickness of a solid electrolyte pellet, R is the resistance, and A is the area of the pellet.

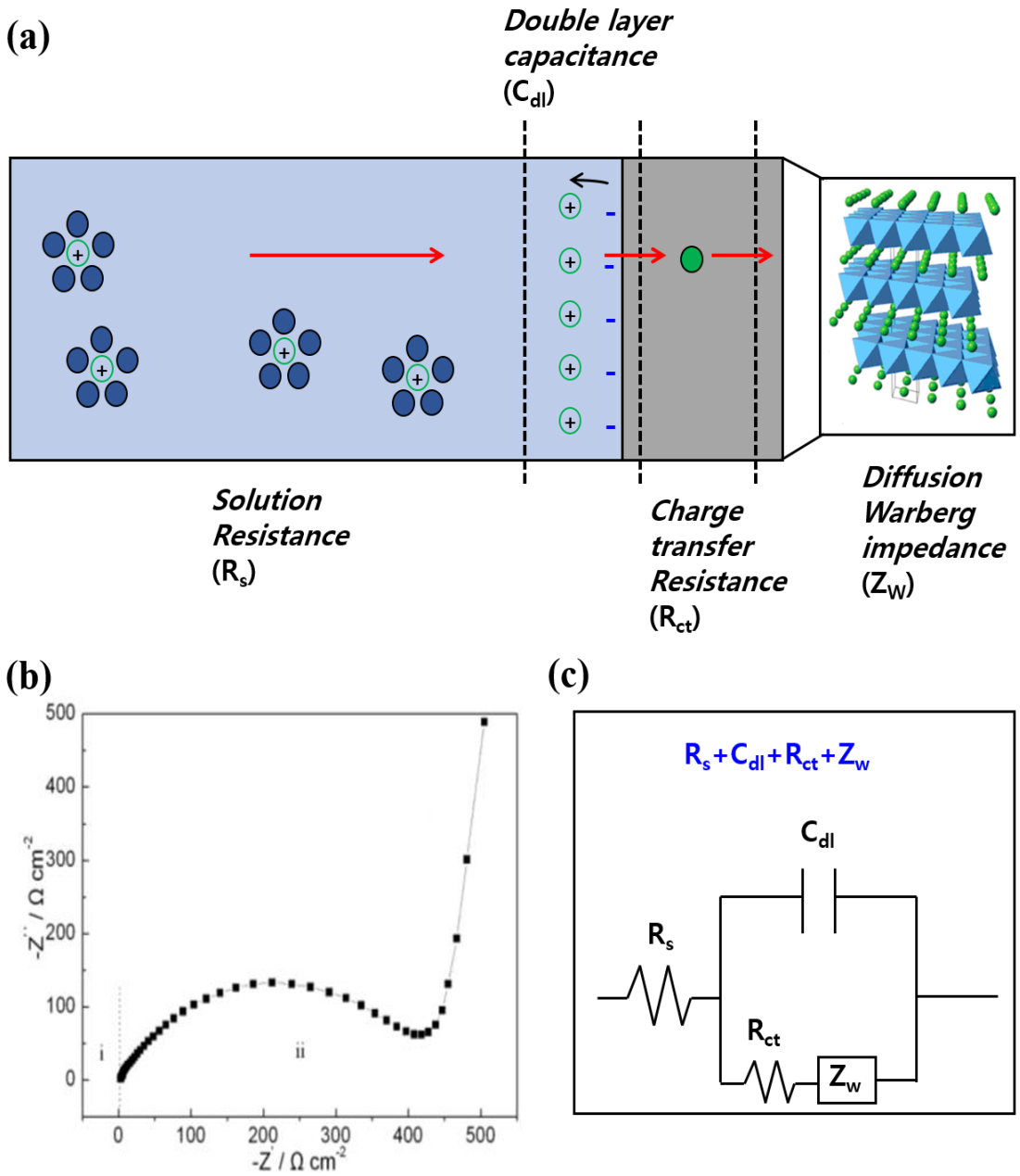


**Figure 2.2** The $Li^+$ diffusion mechanism of lithium ion batteries (a) Nyquist plot of an electrode (b) and equivalent circuit from the Nyquist plot (c).

## 2-2-2. Cyclic voltammetry (CV)

Cyclic voltammetry is typical technique that the current flow can be measured by controlling the potential of the working electrode. This method is a principle of observing the change of current while applying voltage at a constant scan rate (mV/s). This electrochemical analysis provides many information such as the oxidation and reduction mechanism of a material, reversibility from the voltage gap of oxidation and reduction, and reactivity from area of current x voltage [5 - 7]. The measurement can also calculate the diffusion coefficient of lithium ions diffused into an active material through a current change that varies with the scan rate [7, 8]. When the cyclic voltammetry applied to solid electrolyte, its purpose is to evaluate the electrochemical stability of solid electrolyte [9, 10]. The configuration of the cell for the cyclic voltammetry is mainly composed by symmetric Li/electrolyte/SUS or Cu (reference/working/counter electrodes) [9]. The stability of the solid electrolyte is evaluated by comparing the current change while the voltage is being scanned at a constant rate. This method is not an accurate for comparing the degree of reaction of the solid electrolytes, but is good at observing the reaction voltage of the electrolytes.

## 2-2-3. Direct current cycling (DC-cycling)

DC-cycling measurement is one of the galvanostatic measurement such as galvanostatic charge-discharge and galvanostatic intermittent titration technique. The simple electrochemical analysis is conducted by applying the constant current to a cell during charge and discharge with time cut off condition. Recently, this measurement has been used to evaluate the electrochemical stability of solid electrolyte materials (versus Li metal Li/SE/Li) [10]. Compare with cyclic voltammetry, DC-cycling is good for comparing electrochemical reactivity as well as resistance of solid electrolytes. When the solid electrolyte reacts with the

lithium metal, the voltage of the cell changes in an increasing direction. The reason of increasing voltage is the resistance by SEI formation. As followed the simple ohm`s law (V=IR), the voltage increases by some resistance factor when the constant current ($mA/cm^2$) is applied. Because other conditions are same, the resistance is considered by SEI formation between solid electrolyte and Li metal like Li/SEI/SE. Conversely, when the voltage is maintained at a constant value, the solid electrolyte material is considered stable with Li metal. The electrolyte may not react with Li metal or form the SEI with very slow rate. In other cases, the solid electrolyte reacts with Li metal at initial cycles and formed stable SEI. Therefore, the voltage changes do not occur after the first few cycles. This analysis is simple but give many information about electrochemical stability of a material.

# References


[1] C. Ladd, “X ray reflection and the Bragg,” *Phys. Educ.*, vol. 21, no. 1, pp. 1–3, 1986.

[2] C. G. Pope, “X-ray diffraction and the bragg equation,” *J. Chem. Educ.*, vol. 74, no. 1, pp. 129–131, 1997.

[3] H. C and H. C, *The basics of crystallography and diffraction*. Oxford University Press, 1997, 2001.

[4] L. H. Sheng, *Nanostructured phosphate-based electrode materials for lithium batteries*. PhD Diss, 2012.

[5] David K Gosser, *Cyclic voltammetry: simulation and analysis of reaction mechanism*, Vol 43. New York: VCH, 1993.

[6] S. P. Kounaves, *Voltammetric techniques*. Handbook of instrumental techniques for analytical chemistry, 1997.

[7] S. B. Tang, M. O. Lai, and L. Lu, “Li-ion diffusion in highly (003) oriented $LiCoO_2$ thin film cathode prepared by pulsed laser deposition,” *J. Alloys Compd.*, vol. 449, no. 1–2, pp. 300–303, 2008.

[8] C. J. Wen and R. A. Huggins, “Thermodynamic and mass transport properties of LiAl” *Mater. Res. Bull.*, vol. 15, no. 9, pp. 1225–1234, 1980.

[9] B. J. Neudecker and W. Weppner, “$Li_9SiAlO_8$: A Lithium Ion Electrolyte for Voltages above 5.4 V,” *J. Electrochem. Soc.*, vol. 143, no. 7, pp. 2198–2203, 1996.

[10] Z. D. Hood, H. Wang, A. Samuthira Pandian, J. K. Keum, and C. Liang, “$Li_2OHCl$ Crystalline Electrolyte for Stable Metallic Lithium Anodes,” *J. Am. Chem. Soc.*, vol. 138, no. 6, pp. 1768–1771, 2016.

# Chapter 3. Effect of water-soluble binders on the synthesis of $Li_{1.3}Al_{0.3}Ti_{1.7}(PO_4)_3$ and silver-modified LATP $Li_{1.3}Al_{0.4}Ag_{0.1}Ti_{1.6}(PO_4)_3$ solid electrolytes

## 3-1. Introduction

The use of energy storage based lithium ion batteries are widely used as power sources in portable electronic devices such as hand phone, laptop, camera, etc [1]. However, the safety issue of the organic electrolyte in batteries causes anxiety and potentially explodes due to its flammability and leaking, thus an alternate replacement is needed which has the same or greater capacity to solve these problems [2]. Rechargeable batteries from all-solid-state lithium ion batteries (ASSLBs) have been developed and attracted attention in the last few decades [3]. The existing solid electrolytes were made from non-flammable and safe materials which can transfer the $Li^+$ ion as well as the organic liquid electrolytes [4 - 6]. Furthermore, ASSLBs with solid electrolytes may replace the currently available lithium-ion batteries (LIBs) and will be produced on a large scale for commercial use.

Various types of inorganic solid electrolytes, such as sulfide-type, garnet-type, anti-perovskite-type, LISICON-type, and NASICON-type have been investigated extensively. The NASICON-type $Li_{1+x}Al_xTi_{2-x}(PO_4)_3$ (LATP) formed from previous $LiTi_2(PO_4)_3$ structure, which has a rhombohedral structure with a space group of R-3c and composed by $TiO_6$ octahedron and $PO_4$ tetrahedron, which are connected by their angles to form a three-dimensional (3D) network structure. This connection causes cavities where Li-ions reside and bottlenecks in which Li-ions pass through [7 - 10]. By now, LATP solid electrolyte known as an air-stable material with oxidation, chemical, and thermal stability than sulfide solid electrolyte [11]. Hence, LATP solid electrolyte can be used and further developed for lithium

batteries because it has good water stability and a promising electrolyte material for the next-generation aqueous Li batteries [7, 12].

Numerous approaches and strategies have been done in order to increase the ionic conductivity and optimize the capacity of solid electrolytes for battery applications 13 - 19]. Previous work reported the elements doping of LATP with another metal content (Fe[12], Y[19], Cr[20], W[21], and so on) and polymeric composite (PEO[22], PVDF[23], PAN[24], and so on) to enhance the performance of LATP. Aono et al [25, 26] used polyvinyl alcohol (PVA) as a binder to increase the ionic conductivity of LATP solid electrolyte similar to PAA (polyacrylic acid) and CMC (carboxyl methyl cellulose) for solid electrolyte interphase [27]. In addition, Silver has been used to dope LATP [28], $Li_4Ti_5O_{12}$ [29], and $Li_{0.5}La_{0.5}TiO_3$ [30] to increase the performance of the substrate material, as well as the application for Silver batteries [31]. In this study, two strategies are investigated to obtain the stable material, with addition of water-soluble binders such as PVA, CMC, PAA, and silver modification LATP for the preliminary study. The best binders will further use for electrochemical performance for all-solid-state lithium ion batteries such as cyclic voltammetry and DC-cycling.

## 3-2. Experimental

3-2-1. Preparation of electrolyte

The NASICON-type LATP and LATP with silver modifications were synthesized using a modified solid-state method according to Aono, et al [25]. The raw materials of $Li_2CO_3$ (99.0%≥, Sigma-Aldrich), $Al_2O_3$ (activated, basic, Brockmann I, Sigma-Aldrich), $TiO_2$ (99.8%, Sigma-Aldrich), $(NH_4)_2HPO_4$ (98.0%≥, Sigma-Aldrich), and $AgNO_3$ (99.0%≥, Sigma-Aldrich) were weighted with stoichiometric amounts (10% excess of $Li_2CO_3$ was used) to synthesize the silver-modified $Li_{1.3}Al_{0.3}Ti_{1.7}(PO_4)_3$ electrolyte. The chemical reaction of LATP and silver-modified LATP described in the chemical reactions below. Figure 3.1 shows the schematic

procedure of LATP and silver-modified LATP synthesis. First, all materials were weighted and stirring 600 rpm with 40 mL of ethanol for 1 hour to homogenize the material in solution. After it was uniformly dissolved, the solution was dried in 80°C oven for over 18 hours, calcined at 850°C for 2 hours. The dried material was ball-milled for 2 hours at 400 rpm with ethanol as a solvent and 25 zirconia balls with 10mm diameters. The mixture of the material was dried again in oven to evaporate the volatile compound and calcined at 850°C for another 2 hours. The green powder was formed and ball-milled at 400 rpm for 6 hours. Finally, the powder was pressed into a pellet with the addition of 1% PVA binder. Then, the mixed electrolyte was pelletized with 300 bar pressure and sintering at 900°C for 6 hours. The same procedure was adopted with 1% CMC and 1% PAA binders. The as-synthesized pellets were ground into a fine powder and will further used for electrochemical impedance spectroscopy measurement.

Stoichiometric reaction of LATP and silver-modified LATP $Li_{1.3}Al_{0.4}Ag_{0.1}Ti_{1.6}(PO_4)$:

- **$Li_{1.3}Al_{0.3}Ti_{1.7}(PO_4)_3$**

  $0.65Li_2CO_3 + 0.15Al_2O_3 + 1.7TiO_2 + 3(NH_4)_2HPO_4 \rightarrow Li_{1.3}Al_{0.3}Ti_{1.7}(PO_4)_3 + 6NH_3 + 4.5H_2O + 0.65CO_2$

- **$Li_{1.3}Al_{0.3+x}Ag_xTi_{1.7-x}(PO_4)_3$**

  $0.65Li_2CO_3 + 0.2Al_2O_3 + 0.1AgNO_3 + 1.6TiO_2 + 3(NH_4)_2HPO_4 \rightarrow Li_{1.3}Al_{0.4}Ag_{0.1}Ti_{1.6}(PO_4)_3 + 6NH_3 + 4.45H_2O + 0.65CO_2 + 0.1HNO_3$

  x = amount of Ag content to the chemical compound

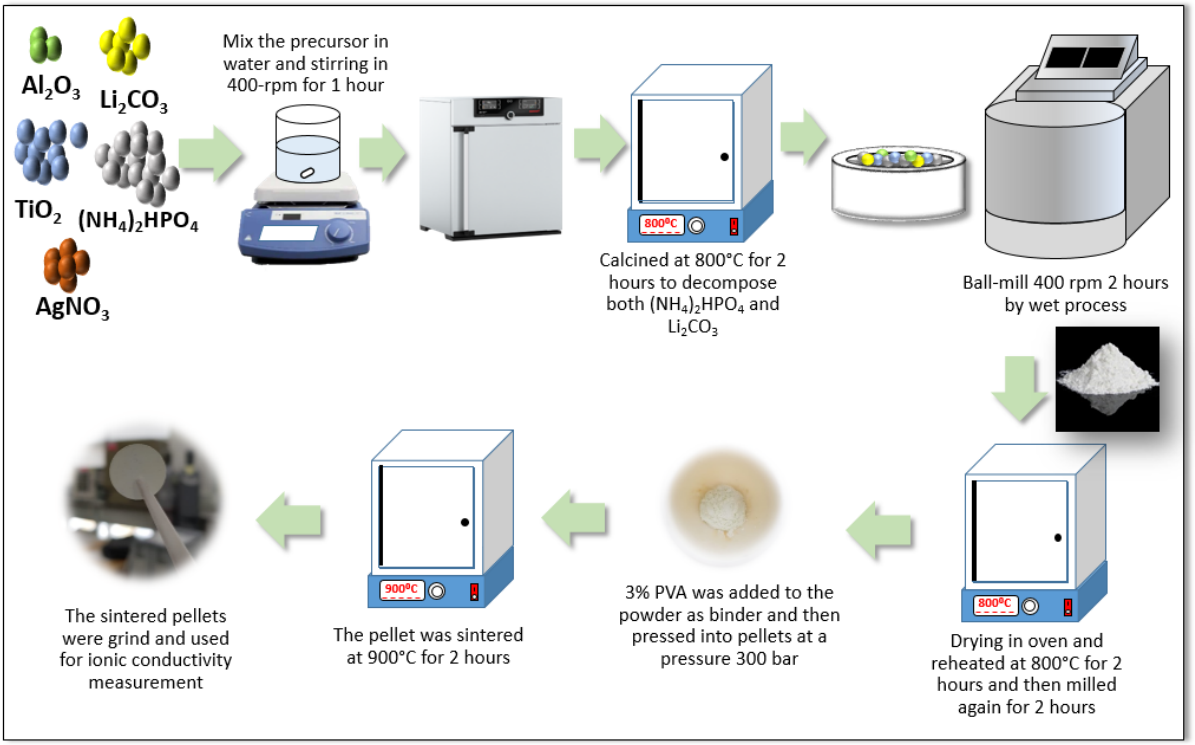


**Figure 3.1** Schematic illustration for synthesis procedure of LATP and silver-modified LATP solid electrolyte.

## 3-2-2. Material characterization

The crystallographic structure of LATP and silver-modified LATP $Li_{1.3}Al_{0.4}Ag_{0.1}Ti_{1.6}(PO_4)$ electrolytes were measured at University of Ulsan research center using X-ray diffraction (XRD) Rigaku-Ultima (IV) with Cu Kα radiation (1.5418 Å) in the 2θ range from 10°-80° with step size of 0.01°. The morphology and elemental analysis of these electrolytes were characterized by a field emission scanning electron microscopy (FE-SEM, JSM-7610F, Japan) and energy dispersive spectroscopy (EDS) with an accelerating voltage of 10kV in order to find the distribution of elements in the solid electrolyte materials.

## 3-2-3. Cell Assembly

The electrochemical measurement of LATP and silver-modified LATP $Li_{1.3}Al_{0.4}Ag_{0.1}Ti_{1.6}(PO_4)$ solid electrolytes were conducted by using CR-2032 coin cell. The composition of the coin cell is composed based on the purpose of the measurements. The LATP and silver-modified LATP $Li_{1.3}Al_{0.4}Ag_{0.1}Ti_{1.6}(PO_4)$ pellets for electrochemical measurements were prepared by pressing the pellet at 300 bar for about 5 minutes with 0.25g of pellet (for Cyclic voltammetry and DC-cycling). Symmetric cells were assembled by stacking LATP between two lithium foils (for DC-cycling) and one lithium foil on one side for CV in a 2032-type coin cell and a spring was added to improve the contact between the LATP and lithium/indium foils (Nilaco, 50 μm thickness) on a both side.

### 3-2-4. Electrochemical analysis

The electrochemical analysis was conducted by Electrochemical Impedance Spectroscopy (EIS), Cyclic Voltammetry (CV) and DC-cycling. Electrochemical impedance spectroscopy (EIS) measurements were conducted using SP-300 (Neo-science, France) instrument over the frequency range of 7 MHz to 0.1 Hz with an amplitude of 50 mV to measure the ionic conductivity of the electrolytes. Solid electrolytes were fabricated by In | solid electrolyte | In symmetric cell using 0.25 g of the material and pressed at 300 bar into pellet using press cell mold (Figure 3.2) with 10 mm diameter and In foil on both sides. Cyclic voltammetry was measured in the coin cell with lithium foil as a reference electrode and SUS plate (stainless steel, 1 t thickness) as a counter electrode using WonATech cycling system. The cell was fabricated with SUS (stainless steel) | solid electrolyte | Li foil order at a scan rate of 1 mV/s and potential window of -0.5 V until 5 V at room temperature. In order to improve the Li transfer through oxide solid electrolytes, the small wet able amount of organic electrolyte was added to the pellet. The solid electrolyte pellet was wetted with a small amount of liquid electrolyte of 1M LiPF6 in ethylene carbonate and dimethyl carbonate (EC : DMC, 1:2 in percent volume) + 2wt% VC to reduce the interfacial impedance between the electrode material and the solid electrolyte [15]. The liquid electrolyte used was approximately 6μL on both side of pellets. 0.25 g of solid electrolytes were compressed into pellet at 300 bar and then lithium foil and SUS plate were attached on a both side of pellets to assemble the cell, respectively.

DC-cycling was carried out with the structure of Li | LATP | Li using WBCS3000 battery tester (WonATech, Korea) and a symmetric cells were assembled by stacking LATP between two lithium foils in a 2032-type coin cell and then SUS (0.5 t thickness) and spacer was added to improve the contact between LATP and lithium foils. 0.25 g of solid electrolyte was compressed at 300 bar using 10 mm diameter mold. After that, the pellet was take out and assemble according to the order as shown in Figure 3.2.

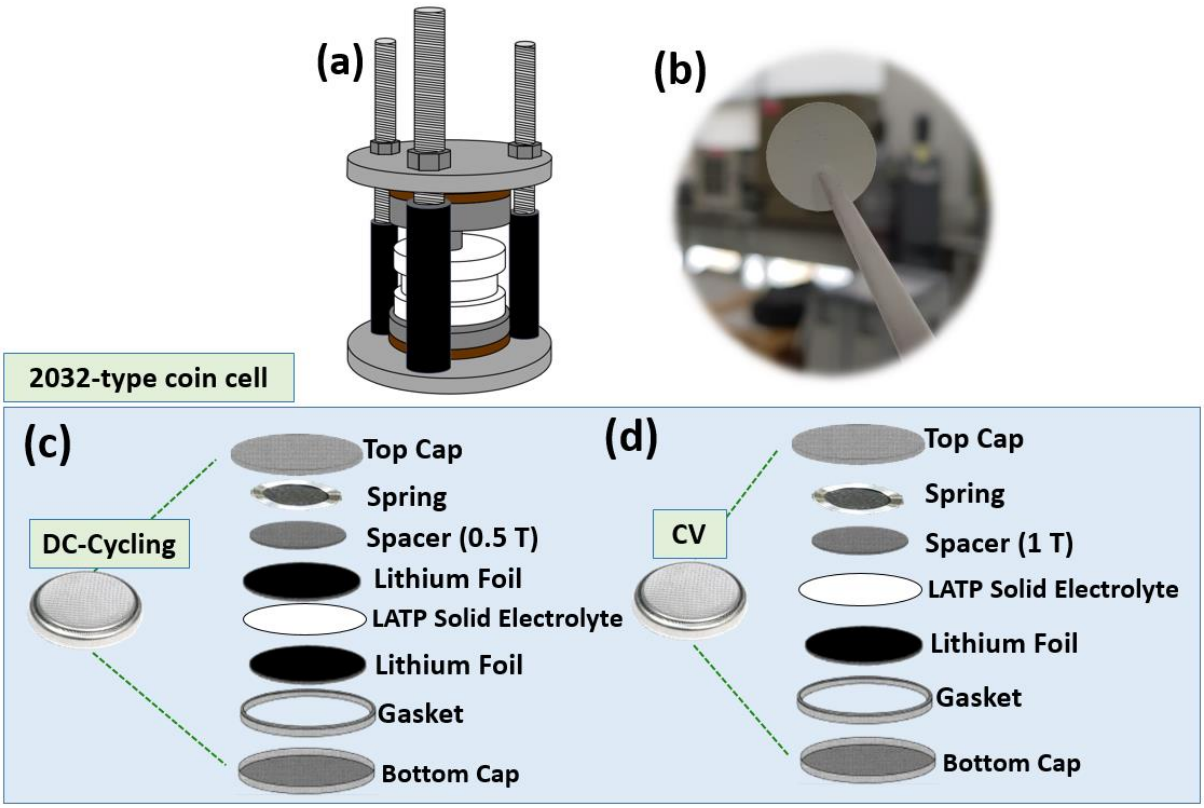


**Figure 3.2** Schematic illustration of (a) press cell for EIS (b) Solid electrolyte pellet, and coin cell assembly configuration for (c) cyclic voltammetry and (d) DC-cycling.

## 3-3. Results and discussion

### 3-3-1. Effect of water-soluble binders on $Li_{1.3}Al_{0.3}Ti_{1.7}(PO_4)_3$ solid electrolytes

#### 3-3-1-1 X-ray Diffraction (XRD) for structural characterization

XRD is useful for determining the crystal structure of a solid sample by measuring the diffraction according to the angle change of the X-ray irradiating the sample. As a result of the experiments, the crystalline phase of as-synthesized LATP with various binders were characterized by XRD analysis. Figure 3.3 is the XRD patterns of NASICON-type LATP before the addition of binders, LATP after addition of binders (PVA, CMC, PAA), and magnified reflections around $2\theta = 33.5°$, respectively. The diffraction peak of pristine LATP and LATP with binders addition are well aligned with $LiTi_2(PO_4)_3$ NASICON structure (PDF 035-0754) with a small impurity peak $LiTiPO_5$ observed as the second phase. It seems like there are no difference changes after the addition of binders to the LATP solid electrolyte. However, the magnified reflections of pristine LATP and LATP with water-soluble binders show a small peak shifting after the addition of the binders. The small concentration of binders cannot be exactly distinguished in LATP pattern since the addition of binders did not change the structure or even the lattice parameters of the LATP. The shifting pattern of XRD may be caused by the different ionic radii or the sample or the lattice condition whether the left-handed shift indicates lattice relaxation and the right-handed shift confirms the strained lattice.

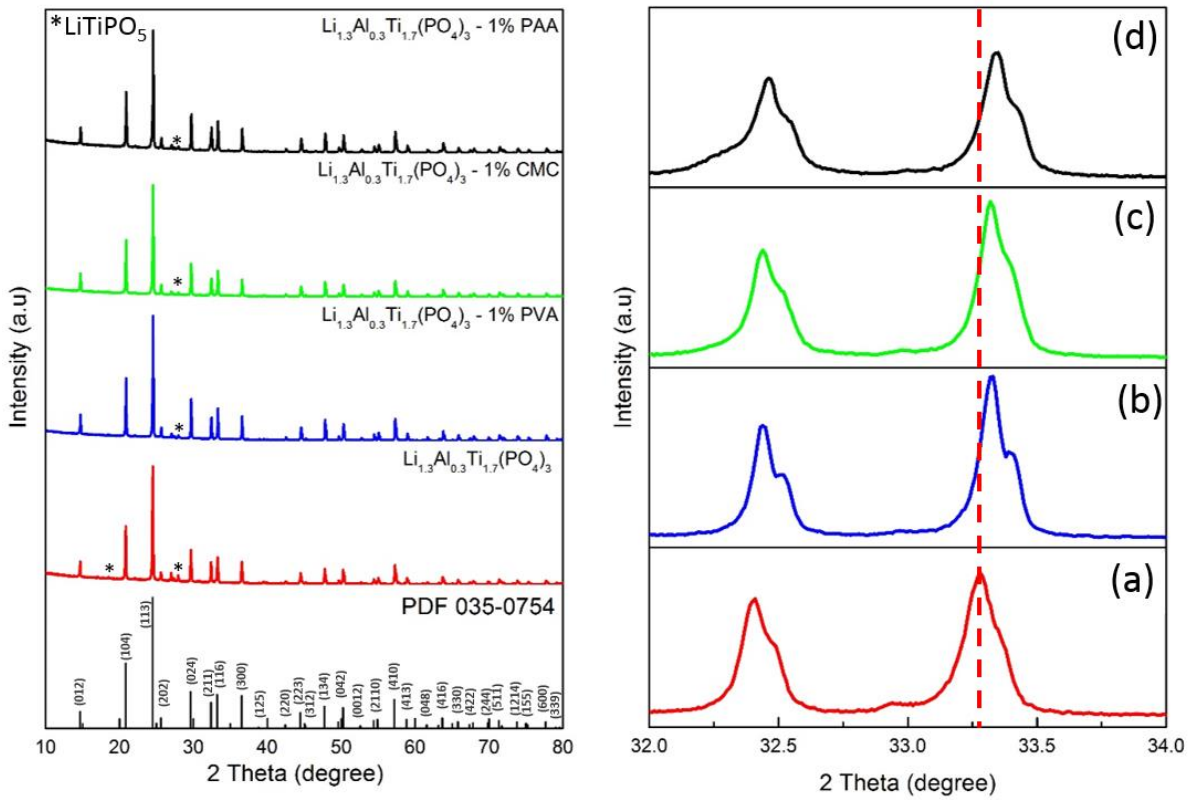


**Figure 3.3** XRD Pattern of LATP ($Li_{1.3}Al_{0.3}Ti_{1.7}(PO_4)_3$) with different water-soluble binders (left) and magnified reflections around $2\theta = 33.3°$ showing a peak shifting from (a) LATP before addition of binders and LATP with water-soluble binders (b) 1% PVA, (c) 1% CMC and (d) 1% PAA. PDF 035-0754 as the reference code of targeted material ($LiTi_2(PO_4)_3$) also attached for comparison.

### 3-3-1-2. SEM and EDS characterization

The combination between surface imaging (SEM) and elemental analysis (EDS) are very useful and robust elemental characterization techniques that widely applied for material and elemental analysis. SEM images and the corresponding EDS elemental mapping of LATP solid electrolyte and water-soluble binders added to solid electrolytes prepared by modified solid-state method are shown in Figure 3.4, displaying the surface morphology of LATP and LATP with PVA, CMC, and PAA binders using SEM with various magnification. The morphologies of the electrolytes show a structure with small particle aggregation. It is obviously seen that the particle size of the particles are ranging from 1 to 10 micrometers. The dispersion and approximate content of the elements constituting the LATP were analyzed by EDS mapping. The weight percentages of EDS mapping also shown in Figure 3.2 (b). Figure 3.2 downside shows that the materials revealed that the constituent elements were well distributed, it implies that successful synthesis of the LATP solid electrolyte with uniform distribution. As shown in EDS mapping, the water-soluble binders are not detected since those binders are only composed of C, H, O constituent only hence it cannot be distinguished exactly.

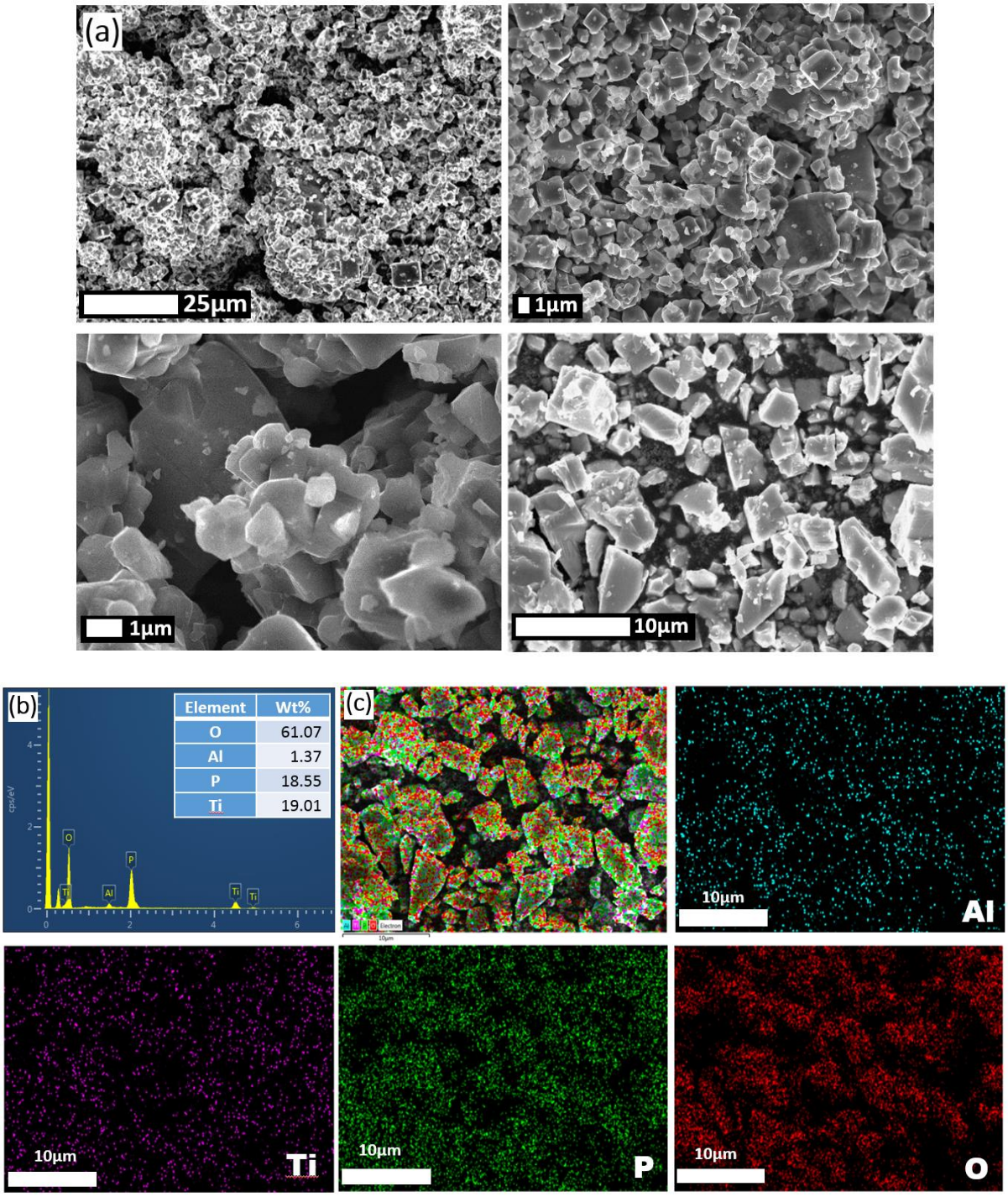


**Figure 3.4** SEM images of (a) $Li_{1.3}Al_{0.3}Ti_{1.7}(PO_4)_3$ solid electrolyte, (b) Mapping results of electrolytes, and (c) EDS mapping of $Li_{1.3}Al_{0.3}Ti_{1.7}(PO_4)_3$ with water-soluble binders with general mapping, Al, Ti, P, and O mapping with 10µm scale images.

### 3-3-1-3. Electrochemical analysis

To study the interfacial resistance between the electrodes and solid electrolytes, we measured the EIS analysis of solid electrolyte in In | solid electrolyte | In symmetric cell over the frequency range of 7 MHz to 0.1 Hz with an amplitude of 10 mV using an SP-300 analyzer at room temperature. Figure 3.5 provides the Nyquist plots of the solid electrolyte using the EIS measurements, which can be used to calculate the ionic conductivity from the resulting resistance in a semi-circle graph. This plot shows a depressed semicircle in the high middle frequency region and a sloping straight line in the low frequency region [32]. Table 3.1 shows the ionic conductivity for LATP solid electrolyte and water-soluble binders added to solid electrolytes. As shown in the table, the ionic conductivity of LATP without the addition of binders has a small value compared to LATP with the addition of binders. The binders take a role in the granulation process and make an electrolyte denser hence increasing the $Li^+$ diffusion to increase the ionic conductivity. The LATP with 1% binders exhibits higher ionic conductivity of 4.65 x $10^{-5}$ S/cm, followed by LATP with 1% CMC with ionic conductivity of 4.21 x $10^{-5}$ S/cm. The small resistance value of the solid electrolytes may be caused by solid electrolyte particle size and crystallinity phase of the electrolyte where these factors can affect the Li transfer diffusion process in the solid electrolyte [33]. Here we can conclude that the addition of binders to the electrolyte increased the ionic conductivity of the electrolyte and this binder's concentration can be optimized with any various concentration.

The electrochemical analysis which provides information such as the oxidation and reduction mechanism of a material, reversibility from the voltage gap of oxidation-reduction and reactivity from the area of current x voltage were conducted using cyclic voltammetry (CV). Figure 3.6 shows the cyclic voltammetry results of the LATP solid electrolyte and water-soluble binders added to the LATP for the symmetric cell Li | solid electrolytes | SUS at a scan

rate of 1mV/s over the potential range -0.5V to 5V (vs. $Li/Li^+$). The cyclic voltammetry results were obtained to understand the electrochemical behavior and stability of the oxidation and reduction process of LATP solid electrolyte. The oxidation peak of the metallic lithium dissolution process ($Li \rightarrow Li^+ + e^-$) can be identified in a range from -0.2V to 0.7V and the reduction peak of the lithium deposition process ($Li^+ + e^- \rightarrow Li$) exist from 0.5V to 0V. However, between -0.5V and 5V (vs. $Li/Li^+$), we cannot find noticeable any other current peak than the reduction/oxidation reactions of metallic lithium. It indicates that the LATP and water-soluble binders added to LATP solid electrolytes have high electrochemical stability due to the wide potential window up to 5V used (vs. $Li/Li^+$) by the shortage of side reactions, and it is confirmed that the electrochemical stability window for LATP is ranging from 2.7V to 4.7 as shown in Figure 1.13 [34]. Among the LATP and water-soluble binders added to LATP, the LATP with 1% CMC shows the highest current response without any side reactions.

DC-cycling is one of simple electrochemical analysis which is conducted by applying the constant current to a cell during charge and discharge with time cut off condition. This galvanostatic cycling performance was performed to confirm the accuracy of the $Li^+$ conduction through reactivity with Li metal of the solid electrolytes and the electrochemical stability. The symmetric cell of Li/electrolyte/Li is used applying a constant direct current of 1.0 mA $cm^{-2}$ at room temperature for 100 hours. Figure 3.7 shows the galvanostatic cycling curves of the solid electrolytes. This oxide material is not completely stable with Lithium metal which is attributed to decomposing the product and cause a small unstable cycle. As shown in the figure, a small voltage increased observed of LATP solid electrolyte. In addition, LATP with an addition 1% PVA and 1% CMC show not only great cyclability but also high voltage retention. This reason is due to the stable SEI from LATP and it can bring about great stability and the smallest voltage changes which means that it is possible to make stable cells from this solid electrolyte.

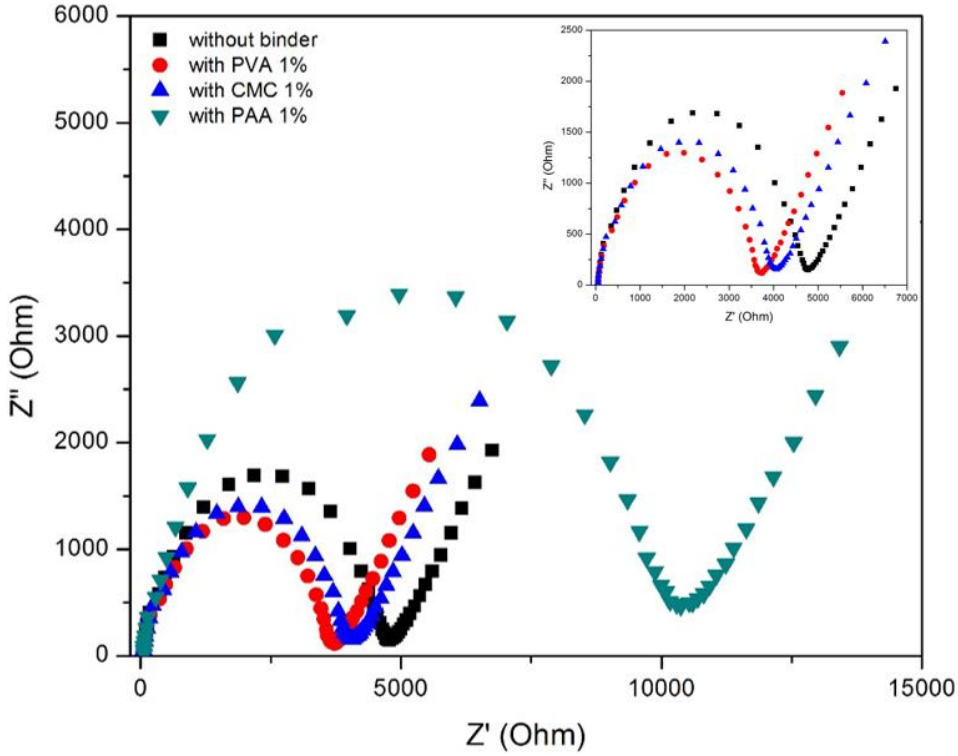


**Figure 3.5** Nyquist plot of $Li_{1.3}Al_{0.3}Ti_{1.7}(PO_4)_3$ with various binders in In | solid electrolytes | In symmetric cell at room temperature.

**Table. 3.1** Ionic conductivity of the solid electrolyte $Li_{1.3}Al_{0.3}Ti_{1.7}(PO_4)_3$ with various binders at room temperature.

| Sample | Resistance (ohm) | Thickness (mm) | $\sigma$ (S $cm^{-1}$) |
|---|---|---|---|
| $Li_{1.3}Al_{0.3}Ti_{1.7}(PO_4)_3$ without binder | 4783 | 1.28 | $3.41 \times 10^{-5}$ |
| $Li_{1.3}Al_{0.3}Ti_{1.7}(PO_4)_3$ with PVA 1% | 3695 | 1.35 | $4.65 \times 10^{-5}$ |
| $Li_{1.3}Al_{0.3}Ti_{1.7}(PO_4)_3$ with CMC 1% | 4022 | 1.33 | $4.21 \times 10^{-5}$ |
| $Li_{1.3}Al_{0.3}Ti_{1.7}(PO_4)_3$ with PAA 1% | 10374 | 1.23 | $1.51 \times 10^{-5}$ |

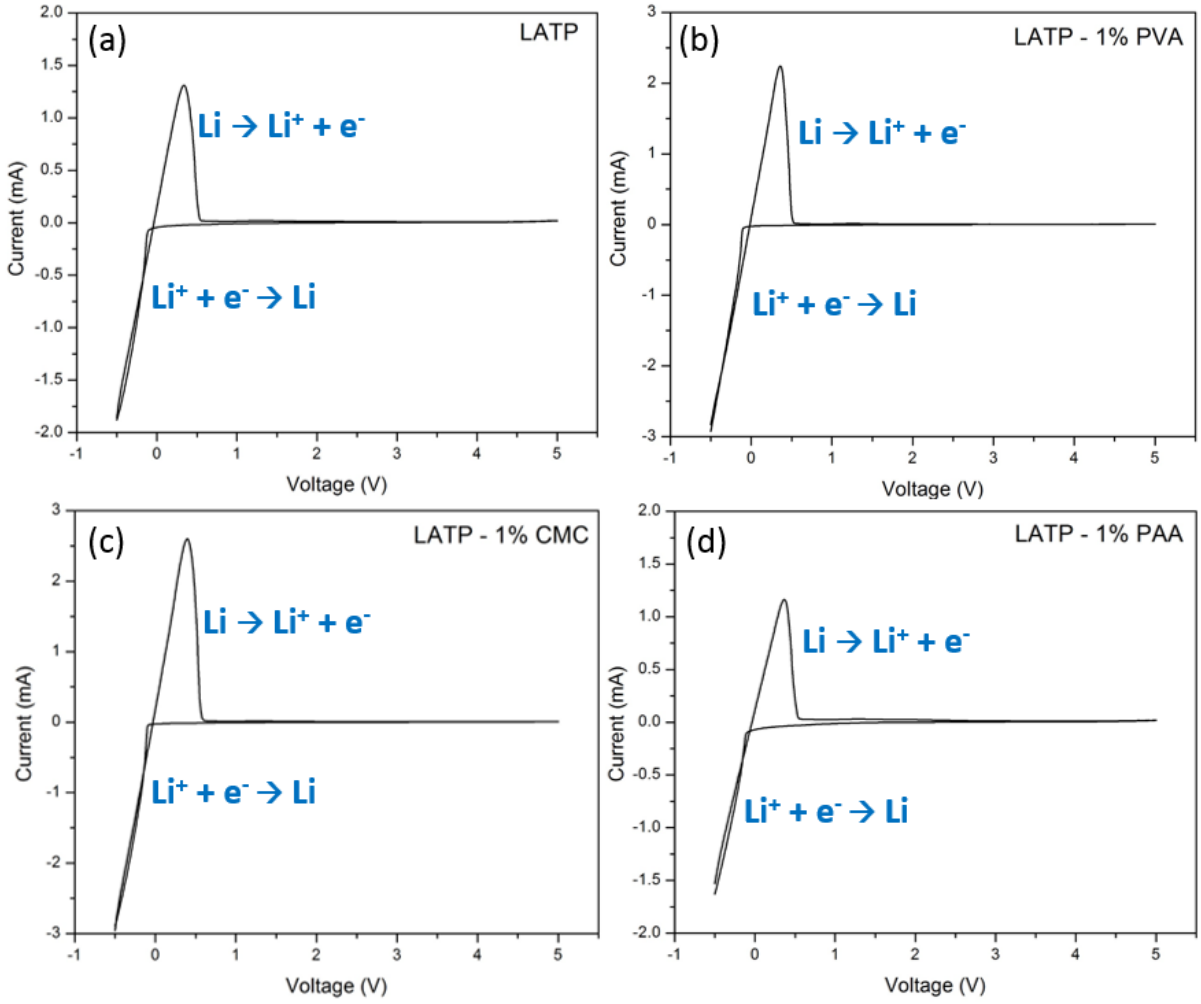


**Figure 3.6** (a-d) Cyclic voltammetry for LATP and water-soluble binders LATP materials at a scan rate of 1mV/s from -0.5 V to 5 V from the Li/electrolyte/SUS cell

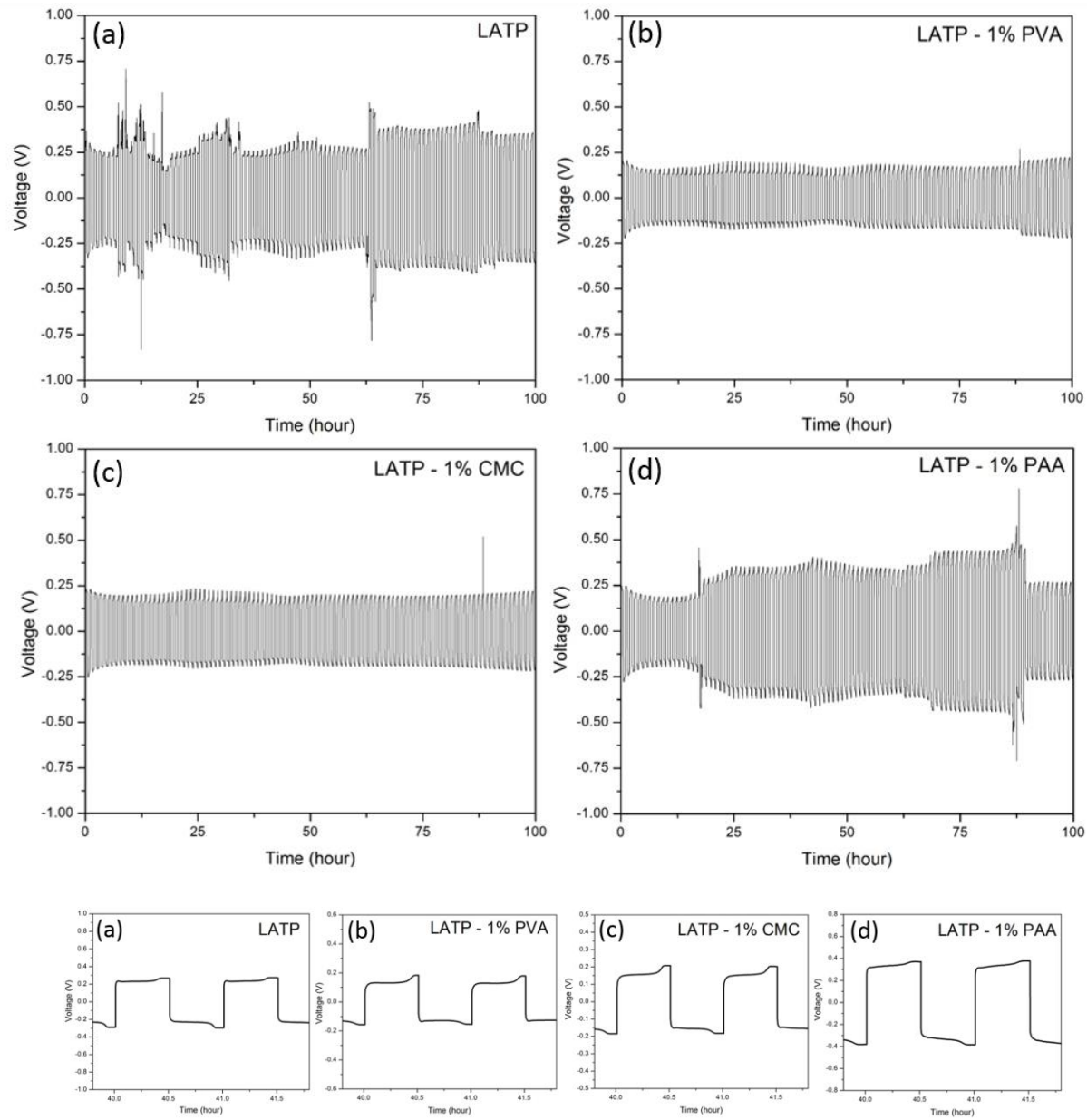


**Figure 3.7** (a-d) Results of DC-cycling test of LATP and water-soluble added to LATP in the symmetric cells Li/solid electrolyte/Li with applied current density of 1 mA $cm^{-2}$ for 100 hours.

### 3-3-2. Effect of water-soluble binders on silver-modified LATP $Li_{1.3}Al_{0.4}Ag_{0.1}Ti_{1.6}(PO_4)_3$ solid electrolytes

### 3-3-2-1 X-ray Diffraction (XRD) for structural characterization

Figure 3.8 shows the comparison of XRD pattern of LATP and silver-modified LATP $Li_{1.3}Al_{0.4}Ag_{0.1}Ti_{1.6}(PO_4)_3$. There is no specific difference of both pattern because of the partial substitution of $Ti^{4+}$ sites with $Ag^{+}$ sites. However, the magnified reflections of both electrolyte show some small different pattern. First, the addition of silver on LATP electrolytes was observed and shows a small increasing intensity peak than the undoped LATP. Second, the new peak was observed around $2\theta = 46.5°$ and little peak broadening at around $2\theta = 32°$ which might be assigned to the effect of silver addition. The peak shifting of the silver-modified LATP $Li_{1.3}Al_{0.4}Ag_{0.1}Ti_{1.6}(PO_4)_3$ is leading to the substitution of $Ti^{4+}$ by $Ag^{+}$ since the ionic radii of $Ag^{+}$ (1.15 Å) is larger than that $Ti^{4+}$ (0.60 Å) and $Al^{3+}$ (0.535 Å) [19, 35] which may be caused the increasing/decreasing the lattice parameter of silver-modified LATP $Li_{1.3}Al_{0.4}Ag_{0.1}Ti_{1.6}(PO_4)_3$. Those results indicating that the Ag was successfully incorporated into the LATP matrix.

Figure 3.9 shows the XRD patterns of silver-modified LATP $Li_{1.3}Al_{0.4}Ag_{0.1}Ti_{1.6}(PO_4)_3$ before the addition of binders, $Li_{1.3}Al_{0.4}Ag_{0.1}Ti_{1.6}(PO_4)_3$ after addition of binders. The diffraction peak of $Li_{1.3}Al_{0.4}Ag_{0.1}Ti_{1.6}(PO_4)_3$ and binders added are well aligned with $LiTi_2(PO_4)_3$ NASICON structure (PDF 035-0754) with a small impurity peak $LiTiPO_5$ observed as the second phase. The small concentration of binders cannot be exactly distinguished in LATP pattern since the addition of binders did not change the structure or even the lattice parameters of the LATP. The shifting pattern of XRD may be caused by the different ionic radii or the sample or the lattice condition whether the left-handed shift indicates lattice relaxation and the right-handed shift confirms the strained lattice.

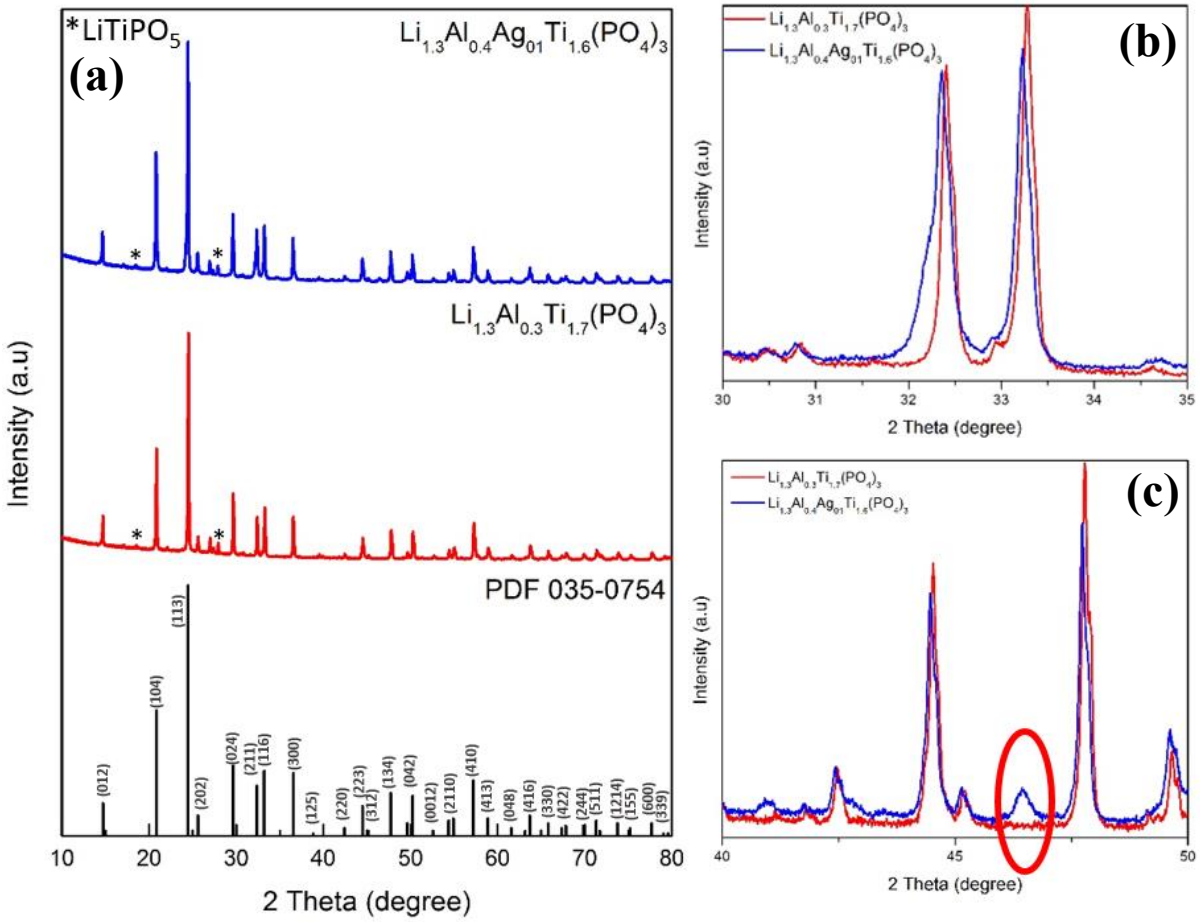


**Figure 3.8** XRD Pattern of LATP ($Li_{1.3}Al_{0.3}Ti_{1.7}(PO_4)_3$) and silver-modified LATP compared to the reference code of targeted material ($LiTi_2(PO_4)_3$) (a). This graph shows that the addition of silver to the LATP material did not show a significant difference with original material, but there is another peak formed at 46-47 theta degree and the addition of silver slightly increase the peak broadening (b-c).

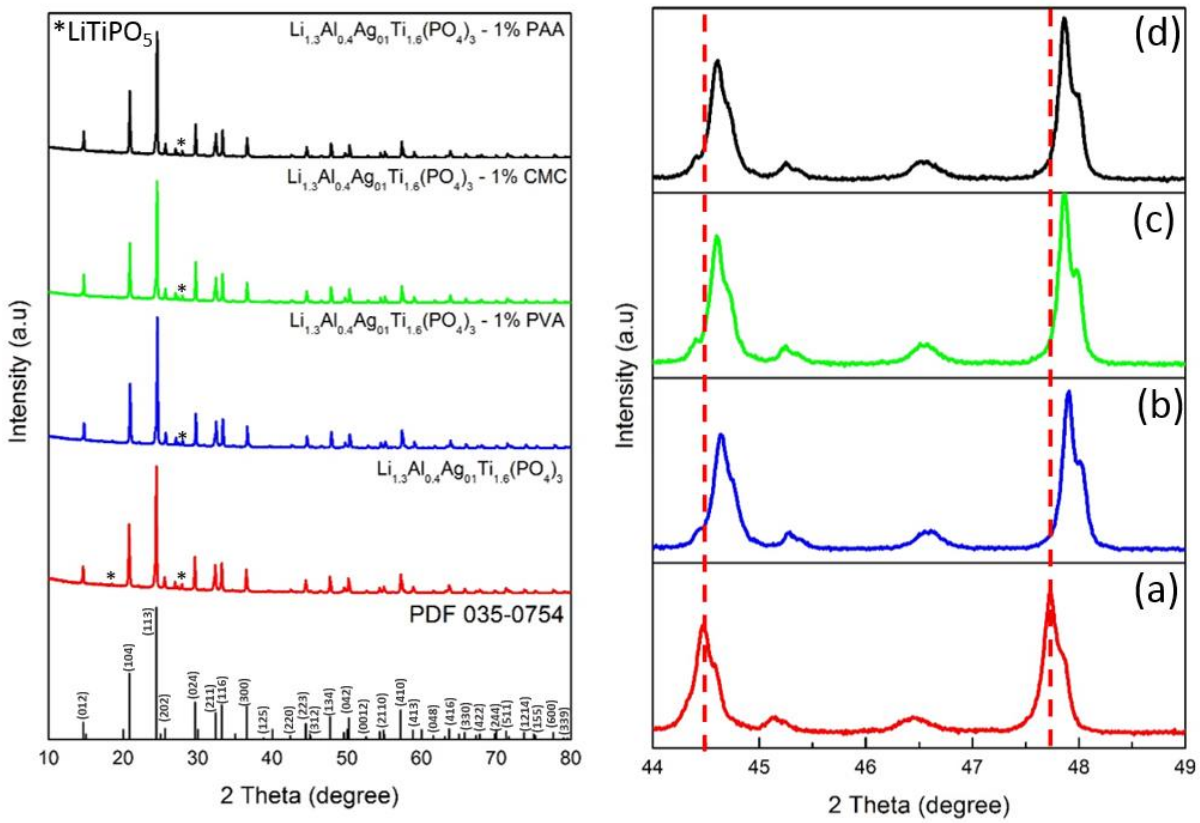


**Figure 3.9** XRD Pattern of silver-modified LATP ($Li_{1.3}Al_{0.4}Ag_{0.1}Ti_{1.6}(PO_4)_3$) with different water-soluble binders (left) and magnified reflections around $2\theta = 44.5°$ and 47.7° showing a peak shifting from (a) $Li_{1.3}Al_{0.4}Ag_{0.1}Ti_{1.6}(PO_4)_3$ and $Li_{1.3}Al_{0.4}Ag_{0.1}Ti_{1.6}(PO_4)_3$ after addition binders of (b) 1% PVA, (c) 1% CMC and (d) 1% PAA. PDF 035-0754 as the reference code of targeted material ($LiTi_2(PO_4)_3$) also attached for comparison.

### 3-3-2-2. SEM and EDS characterization

The SEM and EDS was performed to identify the morphology and size particle of the electrolyte as shown in Figure 3.10 provides the SEM images of $Li_{1.3}Al_{0.4}Ag_{0.1}Ti_{1.6}(PO_4)_3$ and mapping of $Li_{1.3}Al_{0.4}Ag_{0.1}Ti_{1.6}(PO_4)_3$ with binders respectively. The particle size of the electrolyte are ranging from 1 to 10 micrometers. These images show amorphous structure and almost same size each other. The dispersion and approximate content of the elements constituting the LATP were analyzed by EDS mapping. The weight percentages of EDS mapping also shown in Figure 3.2 (b). These both large area and small yellow rectangle are represents the intensity of each compound and convert to weight percent data. The reason why the atomic percentage is different from the chemical composition is probably because of Li atom is not included in the EDS mapping. Figure 3.10 downside shows that the materials revealed that the constituent elements were well distributed. When the degree of dispersion of the elements it compared, it implies that the $Li_{1.3}Al_{0.4}Ag_{0.1}Ti_{1.6}(PO_4)_3$ solid electrolyte has successfully synthesized with uniform elemental distribution. As shown in EDS mapping, the water-soluble binders are not detected since those binders are only composed of C, H, O constituent only hence it cannot be distinguished exactly.

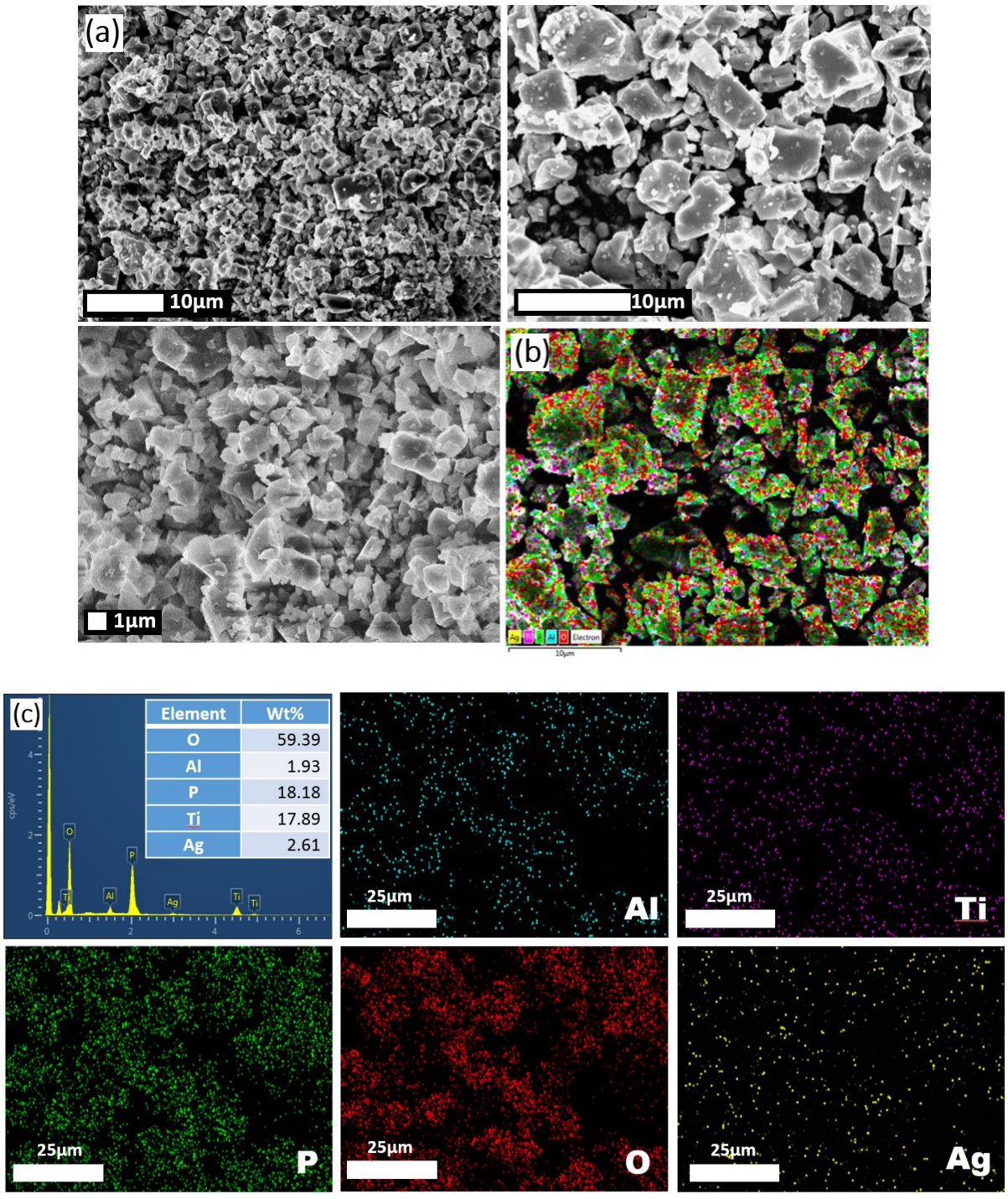


**Figure 3.10** SEM images of (a) $Li_{1.3}Al_{0.4}Ag_{0.1}Ti_{1.6}(PO_4)_3$ solid electrolyte, (b) EDS mapping of $Li_{1.3}Al_{0.4}Ag_{0.1}Ti_{1.6}(PO_4)_3$ with water-soluble binders with general mapping, Al, Ti, P, O, and Ag mapping with 25μm scale images, and (c) Mapping results of the electrolytes.

### 3-3-2-3. Electrochemical analysis

In order to improve the ionic conductivity, various binders were mixed with the solid electrolyte as binders. Figure 3.11 shows the Nyquist plots of samples measured in In | solid electrolytes | In symmetric cells using 10 π sized mold at room temperature. It clearly shows that there is a difference in resistance value after the addition of binders to the $Li_{1.3}Al_{0.4}Ag_{0.1}Ti_{1.6}(PO_4)_3$ and binders added to the electrolytes. The calculated $Li^+$ conductivities of the electrolytes are listed in table 3.2. This measurement adapts the direct measurement without Au coating or sputtering for the blocking effect of the ions, hence the binders were introduced to change the high-cost supporting material to increase the ionic conductivity. However, this value should be increased by reducing the particle size and optimized the addition of binders to the electrolyte hence the ionic conductivity should improve correctly. As shown in the table, the result shows that the $Li_{1.3}Al_{0.4}Ag_{0.1}Ti_{1.6}(PO_4)_3$ with 1% CMC has the highest ionic conductivity by 3.95 x $10^{-5}$ S/cm. In addition, the ionic conductivity of LATP with silver modification did not show a significant increasing the ionic conductivity as high as the original LATP hence this should be evaluated the role of silver in the solid electrolyte. The water-soluble binders thus play a role in binding the electrolyte for the granulation process before sintering and it is proven to increase the ionic conductivity rather than the electrolytes without binders. It is interesting and needed to conduct further study to investigate the optimal amount of binders added and conduct an electrochemical analysis in the coin cell system.

The electrochemical stability of the as-prepared $Li_{1.3}Al_{0.4}Ag_{0.1}Ti_{1.6}(PO_4)_3$ with the addition of various binders were characterized by cyclic voltammetry (CV). The potential interval between oxidation peak and reduction peas is an important parameter to investigate the electrochemical performance. Figure 3.12 shows the cyclic voltammetry of the

$Li_{1.3}Al_{0.4}Ag_{0.1}Ti_{1.6}(PO_4)_3$ solid electrolytes conducted within the potential range of -0.5V to 5V (vs. $Li/Li^+$) at a scan rate of 1mV/s in Li | solid electrolyte | SUS cells. The oxidation peak of the metallic lithium dissolution process ($Li \rightarrow Li^+ + e^-$) can be identified in a range from -0.1V to 0.75V and the reduction peak of the lithium deposition process ($Li^+ + e^- \rightarrow Li$) exist from 1V to 0V. However, between -0.5V and 5V (vs. $Li/Li^+$), we cannot find noticeable any other current peak than the reduction/oxidation reactions of metallic lithium. According to the figure, the $Li_{1.3}Al_{0.4}Ag_{0.1}Ti_{1.6}(PO_4)_3$ is highly stable in the range -0.5V to 5V (vs $Li/Li^+$). Among these electrolytes, $Li_{1.3}Al_{0.4}Ag_{0.1}Ti_{1.6}(PO_4)_3$ with 1% PVA binders shows the highest current response against Li reduction/oxidation and more stable with no broadening peak near to Li reduction/oxidation peak.

Compare with cyclic voltammetry, DC-cycling is good for comparing electrochemical reactivity as well as the resistance of solid electrolytes. To analysis the electrochemical stability and reactivity with Li metal of $Li_{1.3}Al_{0.4}Ag_{0.1}Ti_{1.6}(PO_4)_3$, DC-cycling measurement were conducted by using the symmetric cell of Li/solid electrolyte/Li for $Li_{1.3}Al_{0.4}Ag_{0.1}Ti_{1.6}(PO_4)3$ and water-soluble added to $Li_{1.3}Al_{0.4}Ag_{0.1}Ti_{1.6}(PO_4)_3$ by applying a constant direct current of 1.0 mA $cm^{-2}$ 100 hours. Figure 3.13 shows the galvanostatic cycling curves of the solid electrolytes. As shown in the figure, an unstable cycle at the first 50 hours of $Li_{1.3}Al_{0.4}Ag_{0.1}Ti_{1.6}(PO_4)_3$ was observed, and a small voltage increased observed of $Li_{1.3}Al_{0.4}Ag_{0.1}Ti_{1.6}(PO_4)_3$ with 1% PVA solid electrolyte. In addition, $Li_{1.3}Al_{0.4}Ag_{0.1}Ti_{1.6}(PO_4)_3$ with an addition 1% PAA shows that the cycle is almost stable, which means this electrolyte was almost not reacted with Li metal. These results explain that the $Li_{1.3}Al_{0.4}Ag_{0.1}Ti_{1.6}(PO_4)_3$ with 1% PAA is stable and reacts with Li metal very slowly. From these results, the addition of PAA binders showing better cycle stability among the $Li_{1.3}Al_{0.4}Ag_{0.1}Ti_{1.6}(PO_4)_3$ electrolytes, it can be concluded that the SEI formation was formed very small and remain stable with small voltage changes.

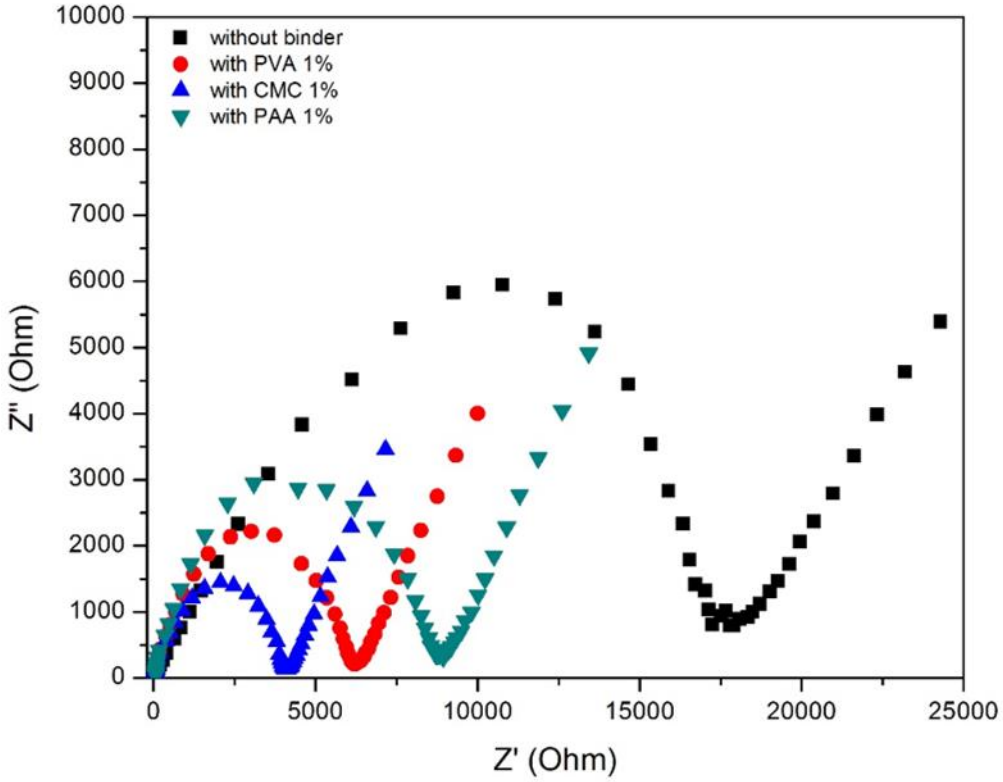


**Figure 3.11** Nyquist plot of $Li_{1.3}Al_{0.4}Ag_{0.1}Ti_{1.6}(PO_4)_3$ with various binders in In |solid electrolytes | In symmetric cell at room temperature.

**Table 3.2** Ionic conductivity of the solid electrolyte $Li_{1.3}Al_{0.4}Ag_{0.1}Ti_{1.6}(PO_4)_3$ with various binders at room temperature.

| Sample | Resistance (ohm) | Thickness (mm) | $\sigma$ (S $cm^{-1}$) |
|---|---|---|---|
| $Li_{1.3}Al_{0.4}Ag_{0.1}Ti_{1.6}(PO_4)_3$ without binder | 17768 | 1.12 | $8.03 \times 10^{-6}$ |
| $Li_{1.3}Al_{0.4}Ag_{0.1}Ti_{1.6}(PO_4)_3$ with PVA 1% | 6216 | 1.25 | $2.56 \times 10^{-5}$ |
| $Li_{1.3}Al_{0.4}Ag_{0.1}Ti_{1.6}(PO_4)_3$ with CMC 1% | 4091 | 1.27 | $3.95 \times 10^{-5}$ |
| $Li_{1.3}Al_{0.4}Ag_{0.1}Ti_{1.6}(PO_4)_3$ with PAA 1% | 8945 | 1.29 | $1.84 \times 10^{-5}$ |

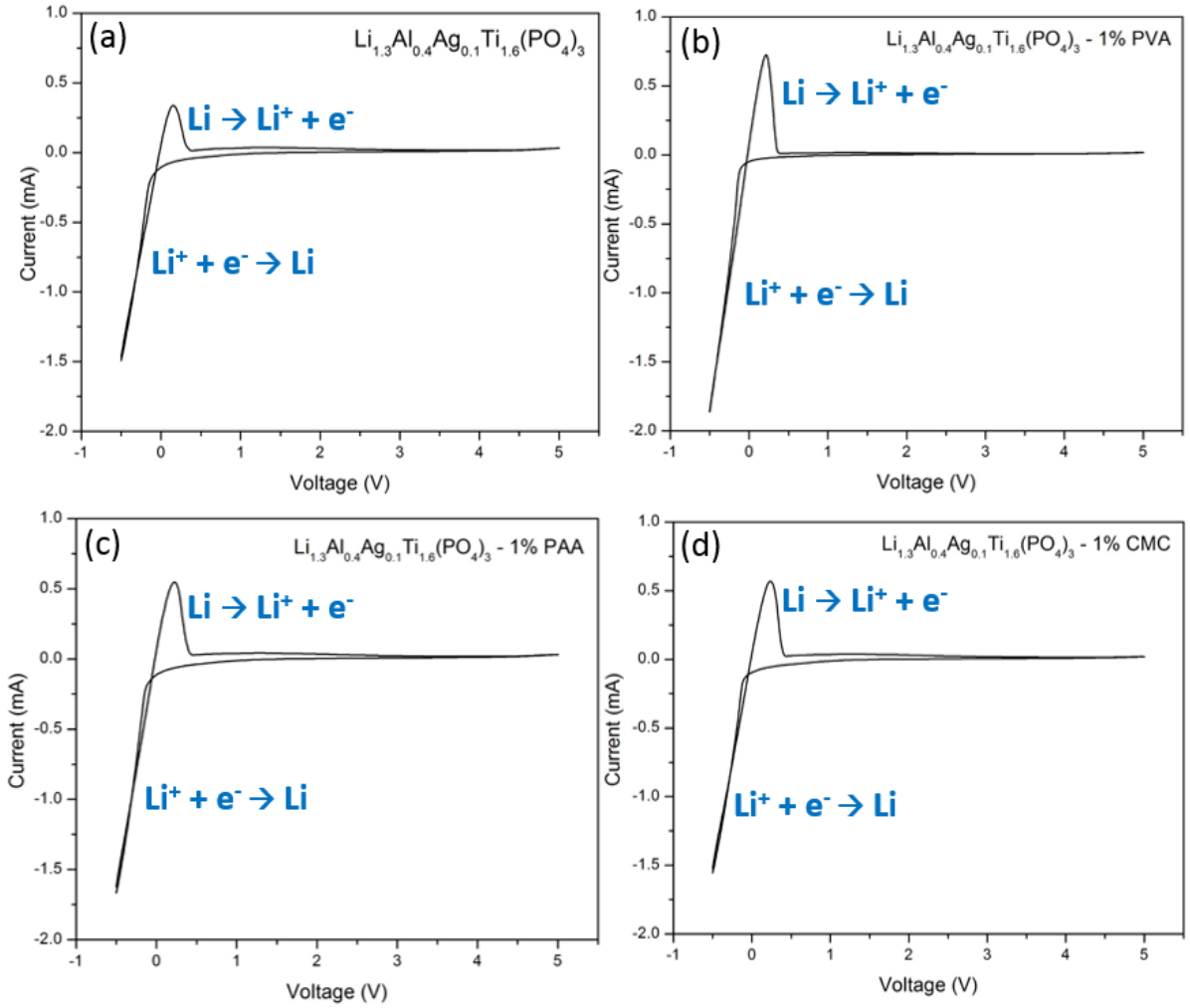


**Figure 3.12** (a-d) Cyclic voltammetry for $Li_{1.3}Al_{0.4}Ag_{0.1}Ti_{1.6}(PO_4)_3$ and water-soluble binders $Li_{1.3}Al_{0.4}Ag_{0.1}Ti_{1.6}(PO_4)_3$ materials at a scan rate of 1mV/s from -0.5 V to 5 V from the Li/electrolyte/SUS cell.

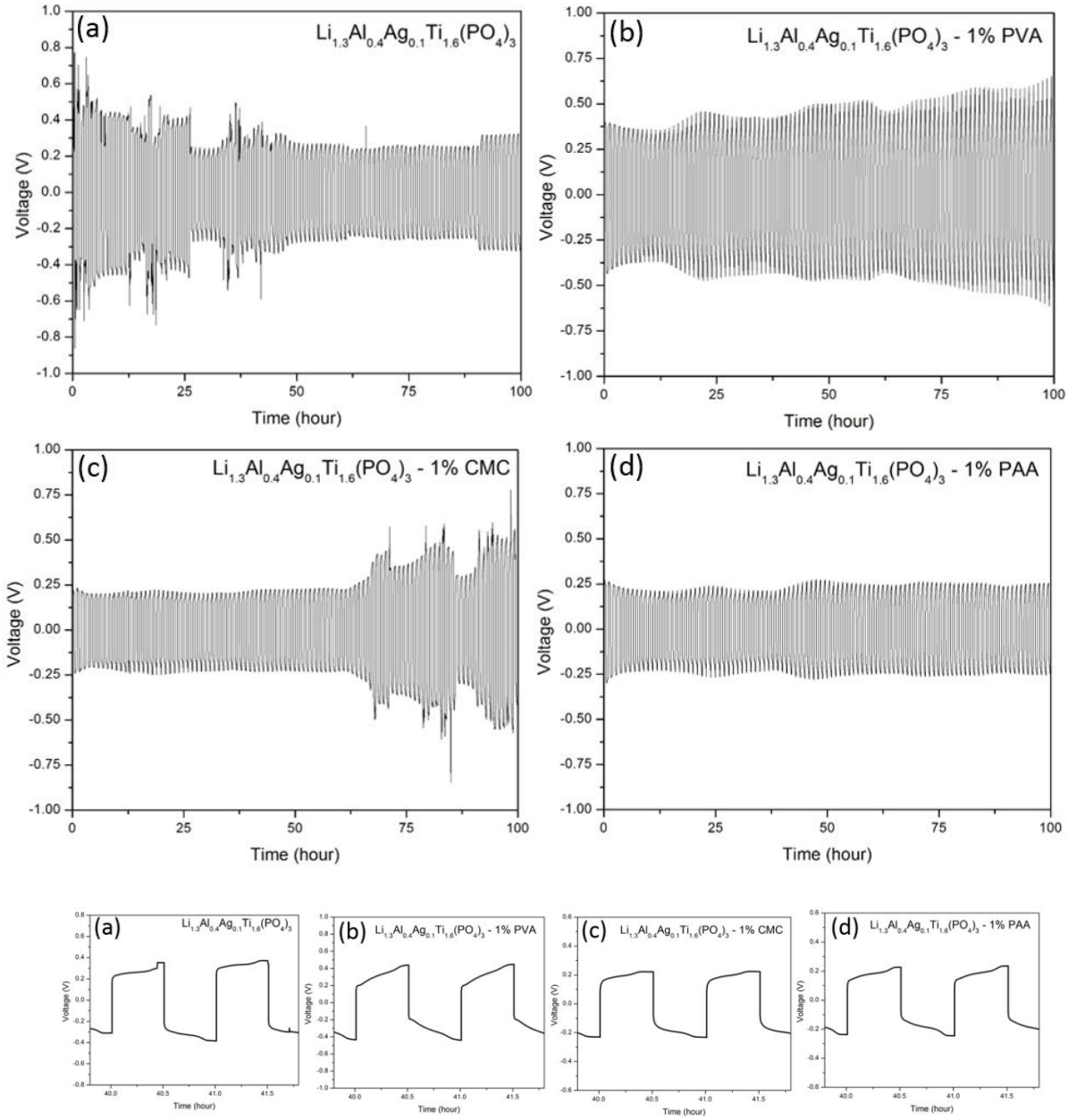


**Figure 3.13** (a-d) Results of DC-cycling test of $Li_{1.3}Al_{0.4}Ag_{0.1}Ti_{1.6}(PO_4)_3$ and water-soluble added to $Li_{1.3}Al_{0.4}Ag_{0.1}Ti_{1.6}(PO_4)_3$ in the symmetric cells Li/solid electrolyte/Li with applied current density of 1 mA $cm^{-2}$ for 100 hours.

# Chapter 4. Conclusion

The NASICON-type LATP and silver-modified LATP $Li_{1.3}Al_{0.4}Ag_{0.1}Ti_{1.6}(PO_4)_3$ solid electrolytes were successfully synthesized with addition of various water-soluble binders using the modified solid-state method. XRD, SEM, and EDS mapping confirmed the structural properties of LATP and silver-modified LATP $Li_{1.3}Al_{0.4}Ag_{0.1}Ti_{1.6}(PO_4)_3$. The binders cannot be detected through XRD and EDS mapping since the small amount quantity and only composed by C, H, and O compounds. The preliminary review of both electrolytes with water-soluble binders was performed using electrochemical impedance spectroscopy (EIS) analysis. LATP with 1% PVA and 1% CMC are currently displaying a comparable value of 4.65 x $10^{-5}$ S/cm and 4.21 x $10^{-5}$ S/c, respectively. Cyclic voltammetry was measured to observed the electrochemical stability of the electrolytes and it revealed that all the electrolyte are stable enough in potential range of -0.5V to 5V (vs $Li/Li^+$). DC-cyclic of LATP and $Li_{1.3}Al_{0.4}Ag_{0.1}Ti_{1.6}(PO_4)_3$ explained that the cycle stability of water-soluble binders shows great cyclability with small voltage increased. At the end, it can be concluded that the addition of water-soluble binders to the electrolyte may increase the ionic conductivity of the electrolyte because of the role of binders to make the electrolyte denser and increase the contact between particles hence increasing the ionic conductivity. For the further, by enhancing the binder contents and performing the electrochemical measurements in the coin cell system, the fascinating importance of high ionic conductivity between LATP and silver-modified LATP $Li_{1.3}Al_{0.4}Ag_{0.1}Ti_{1.6}(PO_4)_3$ will further be explored.

# References


[1] J. Xie and Q. Zhang, “Recent progress in rechargeable lithium batteries with organic materials as promising electrodes,” *J. Mater. Chem. A*, vol. 4, no. 19, pp. 7091–7106, 2016

[2] J. . T. M Armand, “Building better batteries,” *Mech. Eng.*, vol. 139, no. 1, pp. 10–11, 2017.

[3] J. B. Goodenough, “Ceramic solid electrolytes,” *Solid State Ionics*, vol. 94, no. 1–4, pp. 17–25, 1997.

[4] H. Lee, M. Yanilmaz, O. Toprakci, K. Fu, and X. Zhang, “A review of recent developments in membrane separators for rechargeable lithium-ion batteries,” *Energy Environ. Sci.*, vol. 7, no. 12, pp. 3857–3886, 2014.

[5] C. Sun, J. Liu, Y. Gong, D. P. Wilkinson, and J. Zhang, “Recent advances in all-solid-state rechargeable lithium batteries,” *Nano Energy*, vol. 33, no. December 2016, pp. 363–386, 2017.

[6] F. Zheng, M. Kotobuki, S. Song, M. O. Lai, and L. Lu, “Review on solid electrolytes for all-solid-state lithium-ion batteries,” *J. Power Sources*, vol. 389, no. April, pp. 198–213, 2018.

[7] R. DeWees and H. Wang, “Synthesis and Properties of NaSICON-type LATP and LAGP Solid Electrolytes,” *ChemSusChem*, vol. 12, no. 16, pp. 3713–3725, 2019.

[8] H. Y. P. Hong, “Crystal structures and crystal chemistry in the system $Na_{1+x}Zr_2Si_xP_{3-x}O_{12}$,” *Mater. Res. Bull.*, vol. 11, no. 2, pp. 173–182, 1976.

[9] L. Sebastian and J. Gopalakrishnan, “Lithium ion mobility in metal oxides: A materials chemistry perspective,” *J. Mater. Chem.*, vol. 13, no. 3, pp. 433–441, 2003.

[10] J. B. Goodenough, H. Y. Hong, and J. A. Kafalas, “Fast $Na^+$-ion transport in skeleton structures,” vol. I, pp. 203–220, 1976.

[11] A. Manthiram, X. Yu, and S. Wang, “Lithium battery chemistries enabled by solid-state electrolytes,” *Nat. Rev. Mater.*, vol. 2, no. 4, pp. 1–16, 2017.

[12] P. Zhang, M. Matsui, Y. Takeda, O. Yamamoto, and N. Imanishi, “Water-stable lithium

ion conducting solid electrolyte of iron and aluminum doped NASICON-type $LiTi_2(PO_4)_3$," *Solid State Ionics*, vol. 263, pp. 27–32, 2014.

[13] E. Zhao, F. Ma, Y. Jin, and K. Kanamura, "Pechini synthesis of high ionic conductivity $Li_{1.3}Al_{0.3}Ti_{1.7}(PO_4)_3$ solid electrolytes: The effect of dispersant," *J. Alloys Compd.*, vol. 680, pp. 646–653, 2016.

[14] G. B. Kunshina, O. G. Gromov, E. P. Lokshin, and V. T. Kalinnikov, "Sol-gel synthesis of $Li_{1.3}Al_{0.3}Ti_{1.7}(PO_4)_3$ solid electrolyte," *Russ. J. Inorg. Chem.*, vol. 59, no. 5, pp. 424–430, 2014.

[15] J. Liu *et al.*, "Facile synthesis of NASICON-type $Li_{1.3}Al_{0.3}Ti_{1.7}(PO_4)_3$ solid electrolyte and its application for enhanced cyclic performance in lithium ion batteries through the introduction of an artificial $Li_3PO_4$ SEI layer," *RSC Adv.*, vol. 7, no. 74, pp. 46545–46552, 2017.

[16] L. Xingang, T. Jiang, J. Fu, R. Yuan, H. Wen, and C. Zhang, "Facile Synthesis of Nanosized Lithium-Ion-Conducting Solid Electrolyte $Li_{1.4}Al_{0.4}Ti_{1.6}(PO_4)_3$ and Its Mechanical Nanocomposites with $LiMn_2O_4$ for Enhanced Cyclic Performance in Lithium Ion Batteries," *ACS Appl. Mater. Interfaces*, vol. 9, no. 13, pp. 11696–11703, 2017.

[18] S. He, Y. Xu, B. Zhang, X. Sun, Y. Chen, and Y. Jin, "Unique rhombus-like precursor for synthesis of $Li_{1.3}Al_{0.3}Ti_{1.7}(PO_4)_3$ solid electrolyte with high ionic conductivity," *Chem. Eng. J.*, vol. 345, no. 28, pp. 483–491, 2018.

[19] E. Zhao *et al.*, "High ionic conductivity Y doped $Li_{1.3}Al_{0.3}Ti_{1.7}(PO_4)_3$ solid electrolyte," *J. Alloys Compd.*, vol. 782, pp. 384–391, 2019.

[20] P. Zhang *et al.*, "High lithium ion conductivity solid electrolyte of chromium and aluminum co-doped NASICON-type $LiTi_2(PO_4)_3$," *Solid State Ionics*, vol. 272, pp. 101–106, 2015.

[21] X. Lu, F. Meng, S. Huang, and D. Zhao, "Enhanced ionic conductivity and chemical stability of $Li_{1.3}Al_{0.3}Ti_{1.7}(PO_4)_3$ by doping of $WO_3$," *Mater. Lett.*, vol. 230, pp. 177–179, 2018.

[22] X. Ban, W. Zhang, N. Chen, and C. Sun, "A High-Performance and Durable

Poly(ethylene oxide)-Based Composite Solid Electrolyte for All Solid-State Lithium Battery," *J. Phys. Chem. C*, vol. 122, no. 18, pp. 9852–9858, 2018.

[23] X. Shi *et al.*, "Fabrication and electrochemical properties of LATP/PVDF composite electrolytes for rechargeable lithium-ion battery," *Solid State Ionics*, vol. 325, no. April, pp. 112–119, 2018.

[24] Y. Liang, Z. Lin, Y. Qiu, and X. Zhang, "Fabrication and characterization of LATP/PAN composite fiber-based lithium-ion battery separators," *Electrochim. Acta*, vol. 56, no. 18, pp. 6474–6480, 2011.

[25] H. Aono, E. Sugimoto, Y. Sadaoka, N. Imanaka, and G. ya Adachi, "Ionic conductivity and sinterability of lithium titanium phosphate system," *Solid State Ionics*, vol. 40–41, no. PART 1, pp. 38–42, 1990.

[26] O. G. Gromov, G. B. Kunshina, A. P. Kuz'min, and V. T. Kalinnikov, "Ionic conductivity of solid electrolytes based on $Li_{1.3}Al_{0.3}Ti_{1.7}(PO_4)_3$," *Russ. J. Appl. Chem.*, vol. 69, no. 3, pp. 385–388, 1996.

[27] P. Parikh *et al.*, "Role of Polyacrylic Acid (PAA) Binder on the Solid Electrolyte Interphase in Silicon Anodes," *Chem. Mater.*, vol. 31, no. 7, pp. 2535–2544, 2019.

[28] M. Soweizy, M. Zahedifar, and M. Karimi, "Fabrication and characterization of Ag-doped $Li_{1.3}Al_{0.3}Ti_{1.7}(PO_4)_3$ solid electrolyte with high ionic conductivity," *J. Mater. Sci. Mater. Electron.*, vol. 31, no. 12, pp. 9614–9621, 2020.

[29] S. Huang, Z. Wen, X. Zhu, and Z. Gu, "Preparation and electrochemical performance of Ag doped $Li_4Ti_5O_{12}$," *Electrochem. commun.*, vol. 6, no. 11, pp. 1093–1097, 2004.

[30] K. P. Abhilash, P. C. Selvin, B. Nalini, P. Nithyadharseni, and B. C. Pillai, "Investigations on pure and Ag doped lithium lanthanum titanate (LLTO) nanocrystalline ceramic electrolytes for rechargeable lithium-ion batteries," *Ceram. Int.*, vol. 39, no. 2, pp. 947–952, 2013.

[31] Y. G. Guo, Y. S. Hu, J. S. Lee, and J. Maier, "High-performance rechargeable all-solid-state silver battery based on superionic AgI nanoplates," *Electrochem. commun.*, vol. 8, no. 7, pp. 1179–1184, 2006.

[32] F. Gu, G. Chen, and Z. Wang, "Synthesis and electrochemical performances of

$Li_4Ti_{4.95}Zr_{0.05}O_{12}$/C as anode material for lithium-ion batteries," *J. Solid State Electrochem.*, vol. 16, no. 1, pp. 375–382, 2012.

[33] M. Monchak *et al.*, "Lithium Diffusion Pathway in $Li_{1.3}Al_{0.3}Ti_{1.7}(PO_4)_3$ (LATP) Superionic Conductor," *Inorg. Chem.*, vol. 55, no. 6, pp. 2941–2945, 2016.

[34] W. D. Richards, L. J. Miara, Y. Wang, J. C. Kim, and G. Ceder, "Interface Stability in Solid-State Batteries," *Chem. Mater.*, vol. 28, no. 1, pp. 266–273, 2016.

[35] R. D. Shannon, "Revised Effective Ionic Radii and Systematic Studies of Interatomie Distances in Halides and Chaleogenides," *Pharm. Res. An Off. J. Am. Assoc. Pharm. Sci.*, vol. 10, no. 7, pp. 1052–1058, 1993.

# Chapter 4. Summary

We studied the possibility of LATP solid electrolyte and silver-modified LATP $Li_{1.3}Al_{0.4}Ag_{0.1}Ti_{1.6}(PO_4)_3$ with the addition of water-soluble binders such as PVA, CMC, and PAA using a modified solid-state method to improve the ionic conductivity, stability, and electrochemical performance. The structural characterization, surface morphology, and elemental mapping have been observed by XRD, SEM, and EDS. The electrochemical performance of the electrolytes was also measured using EIS, CV, and DC-cycling.

First, we studied the LATP solid electrolyte as the base material in this study. As the results, the LATP has an R3c space group. The electrolyte has an amorphous structure ranging from 1 to 10 μm and the elemental mapping revealed that each element is well uniformed. The ionic conductivity of the LATP electrolyte shows a low ionic conductivity compared to LATP with the addition of water-soluble binders. Second, we compared the original LATP with silver-modified LATP $Li_{1.3}Al_{0.4}Ag_{0.1}Ti_{1.6}(PO_4)_3$ solid electrolytes. After modification with silver, there are no significant changes with the original LATP in terms of ionic conductivity. In addition, the electrochemical stability of $Li_{1.3}Al_{0.4}Ag_{0.1}Ti_{1.6}(PO_4)_3$ in CV and DC-cycling are as stable as pristine LATP and water-soluble binders added to the electrolyte. For water-soluble electrolytes, LATP with 1% PVA and 1% CMC are currently displaying a comparable value of $4.65 \times 10^{-5}$ S/cm and $4.21 \times 10^{-5}$ S/c, respectively. Cyclic voltammetry of the LATP and $Li_{1.3}Al_{0.4}Ag_{0.1}Ti_{1.6}(PO_4)_3$ revealed that all the electrolytes are stable enough in the potential range of -0.5V to 5V (vs $Li/Li^+$). DC-cyclic of LATP and $Li_{1.3}Al_{0.4}Ag_{0.1}Ti_{1.6}(PO_4)_3$ explained that the cycle stability of water-soluble binders shows great cyclability with small voltage increased.